From quasinormal modes of rotating black strings to hydrodynamics of a moving CFT plasma

Luis A. H. Mamani,[1,2,*] Jaqueline Morgan,[3,†] Alex S. Miranda,[2,‡] and Vilson T. Zanchin[1,§]

[1]*Centro de Ciências Naturais e Humanas, Universidade Federal do ABC, Avenida dos Estados 5001, 09210-580 Santo André, São Paulo, Brazil*

[2]*Laboratório de Astrofísica Teórica e Observacional, Departamento de Ciências Exatas e Tecnológicas, Universidade Estadual de Santa Cruz, Rodovia Jorge Amado, km 16, 45650-000 Ilhéus, Bahia, Brazil*

[3]*Instituto Federal de Educação, Ciência e Tecnologia do Rio Grande do Sul, Rua Avelino Antônio de Souza 1730, 95043-700 Caxias do Sul, Rio Grande do Sul, Brazil*

(Received 19 April 2018; published 3 July 2018)

A certain identification of points in a planar Schwarzschild-anti de Sitter (AdS) black hole generates a four-dimensional static black string. In turn, a rotating black string can be obtained from a static one by means of a local boost along the compact direction. On the basis of the gauge/gravity duality, these black strings are dual to rotating thermal states of a strongly interacting conformal field theory (CFT) that lives on a cylinder. In this work, we obtain the complete quasinormal mode (QNM) spectrum of the gravitational perturbations of rotating black strings. Analytic solutions for the dispersion relations are found in the hydrodynamic limit, characterized by fluctuations with wave number and frequency much smaller than the Hawking temperature of the string (or the temperature of the CFT in the dual description). We obtain these dispersion relations both by studying the gravitational perturbations of rotating black strings and by investigating relativistic wave vectors in a moving fluid living on the boundary of the AdS spacetime. Relativistic effects like the Doppler shift of the frequencies, wavelength contraction, and dilation of the thermalization time are shown explicitly in such a regime. The numerical solutions for the fundamental QNMs show a crossover (a transition) from a hydrodynamic-like behavior to a linear relativistic scaling for large wave numbers. Additionally, we find a new family of QNMs which are purely damped in the zero wave number limit and that does not follow as a continuation of QNMs of the static black string, but that appears to be closely related to the algebraically special perturbation modes.

DOI: 10.1103/PhysRevD.98.026006

I. INTRODUCTION

Since its advent in the late 1990s, the celebrated anti-de Sitter/conformal field theory (AdS/CFT) correspondence [1–4] has been extended and applied to different areas of physics. Such developments have lead to what is now known as the AdS/QCD [5–8], the AdS/condensed matter [9–11], and the fluid/gravity [12–14] correspondences. Over the last two decades, the AdS/CFT duality has allowed the study of properties of strongly coupled systems in a n-dimensional flat spacetime by mapping them to a weakly coupled gravitational theory in an asymptotically AdS_{n+1} spacetime. In applications to particle physics, top-down and bottom-up models were used to study, among other things, the mass spectrum, the correlation functions, and the deep inelastic scattering of glueballs, vector and scalar mesons [15–23]. Some phenomena in condensed matter, such as the high-temperature superconductivity [24–26], the classical and quantum Hall effects [27–32] and the (non-)Fermi liquid behavior of certain materials [33–35], were also object of study in the literature. In relation to plasma physics, the fluid/gravity correspondence establishes a one-to-one map between solutions of the relativistic Navier-Stokes equation and asymptotically AdS black hole solutions of Einstein equations [36–40]. Among the important results obtained so far, one may cite the universality of the ratio between the shear viscosity and entropy density of a holographic CFT plasma [41–47].

In the gravity side of the correspondence, the Einstein equations with a negative cosmological constant admit four-dimensional black hole solutions [48,49] with cylindrical horizon topology (see Fig. 1). These objects, known also as black strings, can be put to rotate through a boost in the compact direction, which is an improper coordinate transformation as discussed by Stachel [50]. Although locally equivalent, static and rotating black strings are globally different solutions of the Einstein equations. Just as static black strings are dual to static thermal states of a

*luis.mamani@ufabc.edu.br
†jaqueline.morgan@caxias.ifrs.edu.br
‡asmiranda@uesc.br
§zanchin@ufabc.edu.br

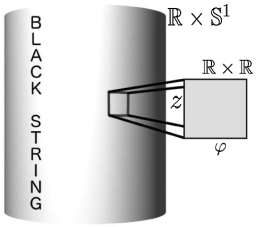

FIG. 1. The global topology of the black string $\mathbb{R}\times\mathbb{S}^1$, and the visualization of the local flat geometry.

strongly coupled CFT on the boundary of the AdS_4 spacetime, the rotating black strings correspond to rotating thermal states of this CFT. Such a theory is defined on a three-dimensional Minkowski spacetime with one compact dimension.

According to the AdS/CFT dictionary, the classical field perturbations in the AdS bulk represent out-of-equilibrium linear excitations in the CFT. In particular, we can obtain finite-temperature correlation functions by evaluating the action of the scalar, electromagnetic, or gravitational perturbations in the AdS spacetime, following the Son-Starinets prescription or its generalizations [51–54]. By explicitly calculating the momentum-space retarded Green's functions in the dual field theory, it has been noticed that the poles of these functions are precisely the frequencies of the quasinormal modes (QNMs) of field perturbations in the AdS spacetime [55–57]. The standard boundary conditions used for asymptotically flat black hole spacetimes are just incoming waves at the horizon and outgoing waves at the spatial infinity, which lead to a complex spectrum for the QNMs [58,59]. In the case of asymptotically AdS backgrounds, the presence of a negative cosmological constant changes the spacetime asymptotic structure and the outgoing wave condition at spatial infinity is, in general, replaced by a Dirichlet boundary condition [60–63].

The study of QNMs of AdS black holes is a two-decade old topic, and so there are a significant number of papers in the literature investigating QNMs in asymptotically AdS spacetimes. See Refs. [64,65] for reviews on the subject and [66–73] for references on the study of QNMs of black branes and black strings. In spite of this long history, the gravitational QNMs of rotating black strings studied in the present work have not been investigated yet. The frequencies of these QNMs correspond to the poles of the stress-energy tensor correlators in the dual CFT. We see that it is possible to separate the gravitational perturbations of the rotating black strings into two sectors, which can be called as transverse and longitudinal perturbations. The main goal of this work is to explore the complete QNM spectrum associated to these perturbations and investigate its connections with the AdS/CFT correspondence.

The structure of the paper is as follows. Section II is a review of the main properties of the rotating black string background, such as the Hawking temperature and the relation with the spacetime of a static black string. In Sec. III the fundamental differential equations for the transverse and longitudinal gravitational perturbations are presented, including a study of the symmetries of these equations. Section IV is dedicated to obtaining the solutions of the fundamental perturbation equations in the hydrodynamic limit. In such an approximation, analytical solutions are found and used to build the dispersion relations for both sectors of the gravitational perturbations. Numerical solutions are also shown for a comparison to the analytical expressions. Several results for nonhydrodynamic QNMs are presented and discussed in Sec. V. Since we cannot find a general exact solution for the differential equations, we use the Horowitz-Hubeny method [60]. Section VI is devoted to investigate the relation between a class of highly damped QNMs and the algebraically special frequencies of the rotating black strings. Section VII contains the final comments and conclusion.

II. THE BACKGROUND SPACETIME

The gravitational background considered here is the spacetime of a rotating AdS_4 black string, whose metric may be written in the form [48]

$$ds^2=\frac{\alpha^2\gamma^2 r_h^2}{u^2}\left[-(dt-ad\varphi)^2 f+\left(\frac{d\varphi}{\alpha}-a\alpha dt\right)^2+\frac{dz^2}{\gamma^2}\right]+\frac{du^2}{\alpha^2u^2f},\tag{1}$$

where α is a parameter related to the AdS radius R by $\alpha=1/R=\sqrt{-3/\Lambda}$, with Λ being the negative cosmological constant, r_h is a constant with units of length, and we defined

$$\gamma=(1-a^2\alpha^2)^{-1/2},\tag{2}$$

$$f\equiv f(u)=1-u^3,\tag{3}$$

with a being the rotation parameter. The ranges of the coordinates are $-\infty<t<+\infty$, $0\le u<\infty$, $0\le\varphi<2\pi$, and $-\infty<z<+\infty$, so that metric (1) represents a rotating black hole with cylindrical topology. In the present coordinates, the AdS boundary, where the dual CFT_3 lives, is located at $u=0$.

The spacetime described by the metric (1) presents an event horizon located at $u=u_h=1$, which is the real positive zero of the equation $f(u)=0$. To establish a relation between the constant r_h and the circumferential radius of the event horizon, we consider the length l of the circular curve of constant t, u, and z, and obtain

$$l=2\pi\frac{\gamma r_h}{u}[1-a^2\alpha^2 f]^{1/2}.\tag{4}$$

In the limit of $u \to u_h$, it follows $l = 2\pi\gamma r_h$, and hence γr_h can be identified with the circumferential radius of the cylindrical surface of the event horizon.

For a rotating black string, the mass M and the angular momentum J per unit length along the string are well defined quantities. In terms of the parameters r_h and a, these quantities are given by [48]

$$M = r_h^3\alpha^3\gamma^2\left(\frac{2+a^2\alpha^2}{8}\right), \qquad J = \frac{3r_h^3\alpha^3 a\gamma^2}{8}. \tag{5}$$

Inverting the last relations, it results in

$$r_h^3 = 2\frac{\sqrt{9M^2-8J^2\alpha^2}-M}{\alpha^3},$$
$$a = \frac{3M-\sqrt{9M^2-8\alpha^2J^2}}{2\alpha^2 J}. \tag{6}$$

As can be seen from the above equations, an event horizon exists if and only if $0 \leq J^2\alpha^2 \leq M^2$, or, equivalently, if and only if $0 \leq a^2\alpha^2 \leq 1$.

The Hawking temperature of a rotating black string can be written as [48]

$$T = \frac{\mathcal{T}}{\gamma}, \tag{7}$$

where $\mathcal{T} = 3\alpha^2 r_h/4\pi$ is the temperature of a static black string with horizon radius r_h. From the dual field-theory perspective, $\mathcal{T}$ is the local rest-frame temperature of the CFT plasma [36,74]. As emphasized by Cardoso *et al.* [75], Eq. (7) "gives the redshift factor relating measurements done in the laboratory and comoving frames".

It is worth mentioning also that the extremely rotating solution is obtained when $a\alpha = 1$, or, equivalently, $J\alpha = M$. In the extremal case, the radius r_h vanishes, which means that the singularity at $u \to \infty$ becomes lightlike. Moreover, the Hawking temperature of the black string vanishes as expected for extremal black holes.

It is important to determine the angular velocity of matter particles and photons around the rotating black strings. In particular, we are interested in obtaining the angular velocity at the event horizon, the static limit surface and the AdS boundary. We start with the general expression for the angular velocity of lightlike particles in a circular orbit (see, e.g., Ref. [76]),

$$\Omega_\pm = \omega_\varphi \pm \sqrt{\omega_\varphi^2 - \frac{g_{tt}}{g_{\varphi\varphi}}}, \tag{8}$$

where

$$\omega_\varphi = -\frac{g_{t\varphi}}{g_{\varphi\varphi}} = \frac{a\alpha^2(1-f)}{1-a^2\alpha^2 f}, \tag{9}$$

and is interpreted as the angular velocity of a locally nonrotating observer [77]. The metric coefficients in Eqs. (8) and (9) are

$$g_{tt} = \alpha^2\gamma^2 r_h^2(a^2\alpha^2 - f)/u^2,$$
$$g_{\varphi\varphi} = \gamma^2 r_h^2(1-a^2\alpha^2 f)/u^2,$$
$$g_{t\varphi} = -a\alpha^2\gamma^2 r_h^2(1-f)/u^2. \tag{10}$$

As it is well known, any timelike particle in a circular orbit is constrained to travel with angular velocity between Ω_+ and Ω_-.

Substituting the metric (1) into Eqs. (8) and (9), we get

$$R\Omega_\pm|_{u=u_h} = a\alpha, \qquad R\omega_\varphi|_{u=u_h} = a\alpha. \tag{11}$$

This is similar to the Kerr and Kerr-Newman black-hole cases, for which the angular velocities $\Omega_\pm$ and ω_φ of equatorial circular orbits coalesce at the horizon. From this we conclude that the angular velocity of the rotating black string is $a\alpha$. The expressions for the angular velocities at the event horizon of rotating charged black strings are found in Refs. [49,78]. Taking the zero charge limit of the expressions presented in those papers, and considering the different notations, we get the results (11).

The stationary limit surface of a rotating black string, defined by the condition $g_{tt} = 0$, is located at $u = u_s = (1-a^2\alpha^2)^{1/3}$. It coincides with the horizon in the nonrotating black string case, when $a\alpha = 0$, and is located outside the horizon for $a\alpha \neq 0$. This means that there is an ergosphere in the rotating black string. On this surface, it results

$$R\Omega_+ = R\omega_\varphi = \frac{2a\alpha}{1+a^2\alpha^2}, \qquad R\Omega_- = 0. \tag{12}$$

Any particle or observer inside the surface delimited by u_s must rotate along the direction of the black string rotation, an effect associated with the inertial frame dragging [77]. In the extremely rotating case ($a\alpha = 1$), $R\Omega_+$ reaches the speed of light. It is worth noticing that the rotating black string has only one event horizon and one stationary limit surface [48], differently from the Kerr black hole, which has event and Cauchy horizons and an ergosphere with two surfaces, the outer surface being located outside the event horizon [79].

At the AdS boundary ($u = u_B = 0$) we get

$$R\Omega_\pm|_{u=u_B} = \pm 1, \qquad R\omega_\varphi|_{u=u_B} = 0. \tag{13}$$

These results show a difference in respect to the asymptotically flat spacetime where the angular velocity vanishes at the spatial infinity as $r\Omega_\pm = \pm 1$, where r is the radial Boyer-Lindquist coordinate. In turn, the result $\omega_\varphi(u_B) = 0$

means that locally stationary observers at the AdS boundary is really at rest.

III. FUNDAMENTAL EQUATIONS FOR THE GRAVITATIONAL PERTURBATIONS

In this section, we present the fundamental differential equations that govern the gravitational perturbations of the background spacetime (1). The starting point is the wave equations for the gravitoelectromagnetic perturbations of rotating charged black strings obtained in Ref. [80]. In the particular case we are interested in here, i.e., for zero electric charge and without source terms, these general differential equations can be written as

$$[f\partial_u(f\partial_u) + \gamma^2(\mathfrak{w} - a\alpha^2\mathfrak{m})^2 - V_{T,L}]\Phi_{T,L} = 0. \quad (14)$$

Here, $\Phi_T(u)$ and $\Phi_L(u)$ stand for the Regge-Wheeler-Zerilli (RWZ) master variables associated, respectively, to the transverse and longitudinal sectors of the gravitational perturbations, while $V_T(u)$ and $V_L(u)$ are the corresponding effective potentials, given by

$$V_T(u) = f(\mathfrak{p}^2 - 3u), \quad (15)$$

$$V_L(u) = \frac{f}{\mathfrak{p}^2 + 3u}\left[\mathfrak{p}^4 + \frac{9(2 + \mathfrak{p}^2u^2 + u^3)}{\mathfrak{p}^2 + 3u}\right], \quad (16)$$

where

$$\mathfrak{p}^2 = \mathfrak{q}^2 + \gamma^2\alpha^2(\mathfrak{m} - a\mathfrak{w})^2. \quad (17)$$

The frequency $\mathfrak{w}$ and the wave numbers $\mathfrak{m}$ and $\mathfrak{q}$ are normalized by the temperature $\mathcal{T}$ according to the relations

$$\mathfrak{w} = \frac{3\omega}{4\pi\mathcal{T}}, \qquad \mathfrak{m} = \frac{3m}{4\pi\mathcal{T}}, \qquad \mathfrak{q} = \frac{3q}{4\pi\mathcal{T}}, \quad (18)$$

where ω is the frequency, m is the wave number along the rotation direction φ, and q is the wave number along the direction z.

In the limit of $a \to 0$, the transverse and longitudinal perturbations, labeled by $(-)$ and $(+)$ in Ref. [80], correspond respectively to the odd (axial) and even (polar) perturbations under the parity transformation $\varphi \to -\varphi$. As shown along this work, the (T) sector gives rise to shear modes in the hydrodynamic regime, while the (L) sector gives rise to sound wave modes.

By comparing Eqs. (14)–(17) to the corresponding differential equations obtained in the static black string case [67,68], we find that the RWZ variables governing the perturbations of a rotating black string satisfy fundamental equations of the same form as the equations for the perturbations of a static black string, provided we consider the change of the radial coordinate r by $u = r_h/r$ and establish the following relation between the frequencies and wave numbers,

$$\begin{cases} \bar{\mathfrak{w}} = \gamma(\mathfrak{w} - a\alpha^2\mathfrak{m}), \\ \bar{\mathfrak{m}} = \gamma(\mathfrak{m} - a\mathfrak{w}), \\ \bar{\mathfrak{q}} = \mathfrak{q}, \end{cases} \quad (19)$$

where the barred and unbarred quantities refer, respectively, to the static and rotating cases. Such a connection between the perturbation equations of a rotating and a static black string are expected in advance, since the metrics of the corresponding background spacetimes are related by an "illegitimate" linear transformation, which mixes the time with the angle φ [48,49]. The same result was obtained in the study of electromagnetic perturbations of rotating black strings [73]. Hence, in principle, the equations of motion for the gravitational perturbations of the rotating black string, Eq. (14), could be obtained directly by replacing relations (19) into the fundamental differential equations for the perturbations of the static black string.

In addition to the fundamental equations, the perturbation problem in an anti-de Sitter spacetime requires the imposition of boundary conditions at the horizon and at the AdS boundary. Whereas the natural boundary condition at $u = u_h$ is that of an ingoing wave only, since classically the horizon acts like a one-way membrane, the boundary condition at the spatial infinity can be Dirichlet, Neumann, or Robin according to which the field perturbations, their derivatives or a combination of both are required to vanish at the anti-de Sitter boundary.

Another important issue in the determination of the quasinormal spectrum of black holes is the choice of appropriate gauge-invariant quantities to describe the perturbations of the black hole. As an example, it is known that the electromagnetic and gravitational QNM spectra of the even (polar) sector, obtained by using the RWZ and Kovtun-Starinets (KS) [63] master variables, are different if one uses the same boundary condition at the spatial infinity (see, for instance, Refs. [70,81]). As first argued in Ref. [81] and elaborated in details in Ref. [82] for a global Schwarzschild-AdS$_4$ black hole, the criterion of nondeformation of the boundary metric requires the imposition of Robin-type conditions on the RWZ master fields. These boundary conditions are translated into Dirichlet conditions for the KS variables [72].

Therefore, to describe gravitational perturbations of AdS backgrounds, the KS variables have at least two advantages over the RWZ variables. The first one is the correspondence between the QNM frequencies and the poles of the stress-energy tensor correlators in the dual field theory [63], which is easier to be established by using the KS than by using the RWZ master functions. The second one is that numerically it is easier to deal with Dirichlet than with Robin boundary conditions.

In this work, we use the KS gauge-invariant quantities, and so it is important to express the fundamental equations of the gravitational perturbations in terms of such variables.

Our task is then to rewrite the differential equations (14) in terms of the KS gauge invariant variables. To do that we need the relations between the RWZ and KS variables as it was done in Ref. [72] for a d-dimensional black brane, which is a topologically trivial version (for $d=4$) of the static black string. Since the form of such relations are quite different depending on the perturbation sector, we consider the transverse and longitudinal sectors separately.

We start with the transverse sector. In this case, the relation between the RWZ and KS variables can be written as

$$Z_T(u) = P_T(u)\partial_u\Phi_T(u) + Q_T(u)\Phi_T(u), \tag{20}$$

where the coefficients are polynomials in u given by

$$P_T(u) = uf, \qquad Q_T(u) = -f. \tag{21}$$

Notice that relation (20) depends only on the holographic coordinate u. Hence, the differential equation for the KS variable Z_T may straightforwardly be obtained by replacing relation (20) into the corresponding equation for the RWZ variable Φ_T, Eq. (14). After some algebraic manipulations, it yields

$$\partial_u^2 Z_T + \left[\frac{\gamma^2(\mathfrak{w}-a\alpha^2\mathfrak{m})^2\partial_u \ln f}{\gamma^2(\mathfrak{w}-a\alpha^2\mathfrak{m})^2 - f\mathfrak{p}^2} - \frac{2}{u}\right]\partial_u Z_T + \left[\frac{\gamma^2(\mathfrak{w}-a\alpha^2\mathfrak{m})^2 - f\mathfrak{p}^2}{f^2}\right] Z_T = 0. \tag{22}$$

Now we consider the longitudinal sector, whose analysis is not straightforward as in the transverse sector, because the relation between the RWZ and KS master functions depends also on the frequencies and wave numbers [72]. In this situation, we can use the relationship connecting the frequencies and wave numbers of static and rotating black strings, cf. Eq. (19), and the relation between the RWZ and KS variables found in the static case. Working out such relations, it follows

$$Z_L(u) = P_L(u)\partial_u\Phi_L(u) + Q_L(u)\Phi_L(u), \tag{23}$$

where the coefficients are given by

$$\begin{aligned} P_L(u) &= -\frac{f^2(u)\mathfrak{p}^2}{\mathfrak{p}^2+3u}, \\ Q_L(u) &= \frac{-\mathfrak{p}^2}{4(\mathfrak{p}^2+3u)^2}\Big\{2u\mathfrak{p}^2[2\gamma^2(\mathfrak{w}-a\alpha^2\mathfrak{m})^2 - 9u] \\ &\quad + 3[4 + 8u^2\gamma^2(\mathfrak{w}-a\alpha^2\mathfrak{m})^2 + u^3(u^3-14)] \\ &\quad + (u^3-4)u\mathfrak{p}^4 + \frac{36u^3\gamma^2(\mathfrak{w}-a\alpha^2\mathfrak{m})^2}{\mathfrak{p}^2}\Big\}. \end{aligned} \tag{24}$$

Hence, manipulating Eqs. (14), (16), and (23) we obtain the fundamental differential equation for the KS master variable of the longitudinal sector,

$$\partial_u^2 Z_L + \frac{\mathfrak{p}^2 Y_1 + \gamma^2(\mathfrak{w}-a\alpha^2\mathfrak{m})^2 Y_2}{uXf}\partial_u Z_L + \frac{\mathfrak{p}^2 Y_3 + \mathfrak{p}^4 Y_4 + 4\gamma^4(\mathfrak{w}-a\alpha^2\mathfrak{m})^4}{Xf^2} Z_L = 0, \tag{25}$$

where we have introduced the coefficients[1]

$$\begin{aligned} X &= 4\gamma^2(\mathfrak{w}-a\alpha^2\mathfrak{m})^2 - (f+3)\mathfrak{p}^2, \\ Y_1 &= 8f^2 + 3(f+3)u^3, \\ Y_2 &= 4(f-3), \\ Y_3 &= -(\partial_u f)^2 f - (5f+3)\gamma^2(\mathfrak{w}-a\alpha^2\mathfrak{m})^2, \\ Y_4 &= (f+3)f. \end{aligned} \tag{26}$$

For numerical purposes it is important to know the singular points and symmetries of the differential equations (22) and (25). Let us start with the transverse-sector differential equation (22). The singularities of this equation are

$$u_0 = 0, \qquad u_1 = 1, \qquad u_3 = \left[\frac{\mathfrak{m}^2\alpha^2 + \mathfrak{q}^2 - \mathfrak{w}^2}{\mathfrak{p}^2}\right]^{1/3}, \tag{27}$$

and all of them are regular singular points. The same happens with the longitudinal-sector differential equation (25), whose regular singular points are

$$u_0 = 0, \qquad u_1 = 1, \qquad u_3 = \sqrt[3]{4}\left[\frac{\mathfrak{m}^2\alpha^2 + \mathfrak{q}^2 - \mathfrak{w}^2}{\mathfrak{p}^2}\right]^{1/3}. \tag{28}$$

The regular nature of the singularities allows us to expand the solutions near these regular singular points. That is the core of the power series method that we use in the numerical procedure of this work.

Finally, let us look at the symmetries of the Eqs. (22) and (25). Both differential equations are invariant under the following (symmetry) transformations,

$$\begin{aligned} &\{\mathfrak{m}, a\} \to \{-\mathfrak{m}, -a\}; \qquad \{\mathfrak{m}, \mathfrak{w}\} \to \{-\mathfrak{m}, -\mathfrak{w}^*\}; \\ &\{\mathfrak{w}, a\} \to \{-\mathfrak{w}^*, -a\}; \qquad \{\mathfrak{q}\} \to \{-\mathfrak{q}\}; \end{aligned} \tag{29}$$

where $\mathfrak{w}^*$ is the complex conjugate of the frequency $\mathfrak{w}$. These symmetry transformations are going to be used when we present the numerical results in the next sections. We split the complex frequency as $\mathfrak{w} = \mathfrak{w}_R - i\mathfrak{w}_I$, so that the imaginary part $\mathfrak{w}_I$ is positive for decreasing perturbations.

[1]There are some typos in the coefficients presented in Eqs. (3.22) and (4.7) of Ref. [72]. Here we write the correct expressions of the coefficients.

With this convention, negative $\mathfrak{w}_I$ would imply instability against linear perturbations, what does not happen for the rotating AdS black strings in four-dimensional spacetimes. Additionally, we choose to fix the signals of a and $\mathfrak{w}_R$ as being positive, such that (for $\mathfrak{q}=0$) the signal of the wave number component $\mathfrak{m}$ indicates the propagation direction of the wave on the cylinder surfaces of constant u, along or contrary to the string rotation. Hence, we present graphs for numerical results in the first and second quadrants of the planes $(\mathfrak{m},\mathfrak{w}_R)$ and $(\mathfrak{m},\mathfrak{w}_I)$. In the case of $\mathfrak{m}=0$, a similar procedure is followed to present the numerical results in terms of the wave number component $\mathfrak{q}$. The symmetric solutions may be obtained using the transformations of Eq. (29).

IV. HYDRODYNAMIC QUASINORMAL MODES

The hydrodynamic approximation is characterized by a regime where the frequencies and wave numbers are much smaller than the local temperature $\mathcal{T}$, i.e., $\mathfrak{w}\ll 1$, $\mathfrak{q}\ll 1$ and $\mathfrak{m}\ll 1$. In such a regime, it is possible to express the dispersion relations $\mathfrak{w}(\mathfrak{m},\mathfrak{q})$ as power series in the wave numbers $\mathfrak{q}$ and $\mathfrak{m}$. In general, the hydrodynamic frequencies are the lowest frequencies in the spectrum of QNMs. The main characteristic of these modes is that the frequency vanishes as the wave numbers go to zero, i.e., $\mathfrak{w}\to 0$ as $(\mathfrak{m},\mathfrak{q})\to 0$.

In this section, we develop a complete analysis of the hydrodynamic quasinormal modes for the transverse sector (also called shear channel), and for the longitudinal sector (also called sound channel). Firstly, we present the analytical results for both sectors, then we solve numerically the differential equations (22) and (25) with the appropriate boundary conditions and, at the end, we compare the numerical and analytical results.

A. Transverse sector—analytical results

Here we start by writing the dispersion relation for the transverse sector (or shear channel) of the static black string, which is characterized by being a purely damped mode [43,68],

$$\bar{\mathfrak{w}}=-\frac{i}{3}(\bar{\mathfrak{q}}^2+\alpha^2\bar{\mathfrak{m}}^2)+\cdots, \tag{30}$$

where the ellipses denotes higher powers of $\bar{\mathfrak{q}}$ and $\bar{\mathfrak{m}}$. In the specific case of the hydrodynamic QNMs, the fact that $\bar{\mathfrak{w}}\to 0$ as $(\bar{\mathfrak{m}},\bar{\mathfrak{q}})\to 0$ allows us to obtain the dispersion relations of the rotating black strings by substituting the relations (19) directly into Eq. (30) and then solving the resulting equations for $\mathfrak{w}$. To do that, we introduce an additional dimensionless parameter λ, that scales the wave numbers as $\mathfrak{m}\to\mathfrak{m}\lambda$ and $\mathfrak{q}\to\mathfrak{q}\lambda$, so that the frequency can be expanded in terms of this parameter as

$$\mathfrak{w}=c_0+c_1(\mathfrak{m},\mathfrak{q})\lambda+c_2(\mathfrak{m},\mathfrak{q})\lambda^2+c_3(\mathfrak{m},\mathfrak{q})\lambda^3+\cdots. \tag{31}$$

We then solve for the coefficients $c_1(\mathfrak{m},\mathfrak{q}), c_2(\mathfrak{m},\mathfrak{q}),\ldots$, order by order in Eq. (30) and set the coefficient $c_0=0$ because the frequency of a hydrodynamic mode goes to zero in the limit $(\mathfrak{m},\mathfrak{q})\to 0$. After re-introducing the original wave numbers (or, equivalently, by setting $\lambda=1$), we obtain the following dispersion relation,

$$\mathfrak{w}=a\alpha^2\mathfrak{m}-\frac{i}{3\gamma}\left(\frac{\alpha^2\mathfrak{m}^2}{\gamma^2}+\mathfrak{q}^2\right)+\cdots. \tag{32}$$

Rewriting Eq. (32) in terms of the non-normalized frequency and wave numbers, it follows that

$$\omega=a\alpha^2 m-\frac{i}{4\pi\gamma\mathcal{T}}\left(\frac{\alpha^2 m^2}{\gamma^2}+q^2\right)+\cdots. \tag{33}$$

The result (33) is the dispersion relation of a diffusion problem, where the first term on the right hand side is the convective term (with velocity $a\alpha$). The coefficient of the quadratic term is the shear-diffusion coefficient, given by $D=1/(4\pi\gamma\mathcal{T})$, while the perturbation damping time is defined as $\tau=1/\omega_I$.

It is worth comparing the above results with those obtained for the static black string [43,68]. Our convention here is that black strings rotate counterclockwise (we called this as the positive direction). The wave number parallel to rotation is $\mathfrak{m}$ and the perpendicular component is $\mathfrak{q}$. After comparing the dispersion relation (30) with the non-normalized version of (33), we see there is a Lorentz contraction of the wavelength $2\pi/(\alpha m)$, i.e., $m=\gamma\bar{m}$. There is also a dilation of the damping time, i.e., $\tau=\gamma\bar{\tau}$. These are expected effects for relativistic systems described in different frames. At last, let us mention that Eq. (32) reduces to the static result, Eq. (30), in the limit of zero angular velocity ($a=0$).

B. Transverse sector—numerical results

In this subsection, we solve numerically the differential equation (22) and compare the resulting quasinormal frequencies to the analytical solution, Eq. (32), obtained in Sec. IV A for the hydrodynamic regime $(\mathfrak{w},\mathfrak{m},\mathfrak{q}\ll 1)$.

The numerical solutions are found by means of the power series method developed in Ref. [60]. We notice that it is difficult to visualize and interpret the numerical results by plotting directly the relations $\mathfrak{w}_R(\mathfrak{m},\mathfrak{q})$ and $\mathfrak{w}_I(\mathfrak{m},\mathfrak{q})$, since the results are three-dimensional graphics. For that reason, we initially split the analysis in two cases, as follows.

First, we look for results with $\mathfrak{m}=0$, i.e., for perturbations propagating along the direction z. The corresponding numerical results are displayed in Fig. 2. In this case the

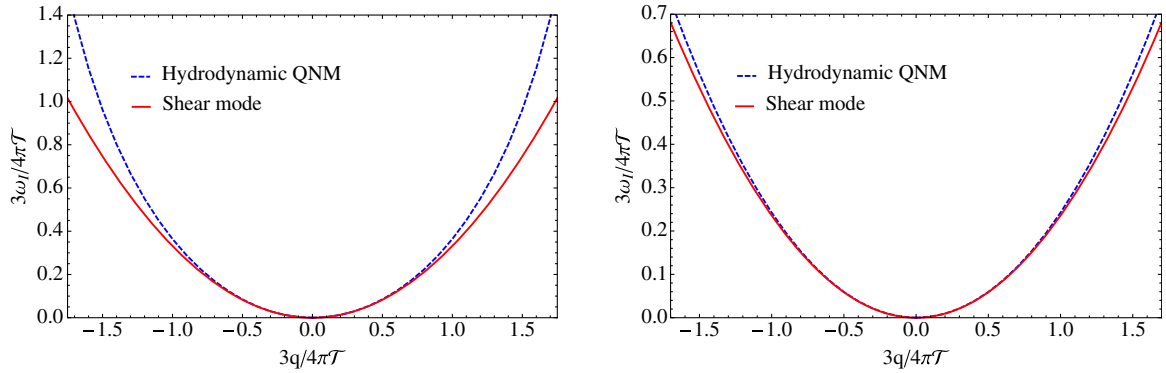

FIG. 2. Dispersion relations of the hydrodynamic QNMs (solid lines), cf. Eq. (32), and shear modes (dashed lines) of the transverse sector, with $\mathfrak{m} = 0$, for $a\alpha = 0.1$ (left panels) and $a\alpha = 1/\sqrt{2}$ (right panel). These solutions are purely damped.

frequencies are pure imaginary numbers. These results are expected because by setting $\mathfrak{m} = 0$ in Eq. (32) the real part of the frequency vanishes. In Fig. 2 the dashed lines represent the numerical results, while the solid lines represent the analytical solution given by Eq. (32). As expected, we observe a good agreement between the numerical and analytical results in the regime of small wave numbers and frequencies. It is also seen that the hydrodynamic approximation is no longer valid for large wave numbers.

The effects of the rotation on the damping time can be noticed in Fig. 2. In fact, it is perceived that, given a specific wave number value, the imaginary part of the frequency for $a\alpha = 0.1$ (left panel) is larger than the imaginary part of the frequency for $a\alpha = 1/\sqrt{2} \approx 0.71$ (right panel). This means that perturbations on a slowly rotating black string are damped faster than the perturbations on a fast rotating black string. In view of the symmetry of the differential equations (14) under the change $\mathfrak{q} \to -\mathfrak{q}$, commented at the end of Sec. III, the curves for negative $\mathfrak{q}$ are mirror-symmetrical to the curves for positive $\mathfrak{q}$.

Second, we look for results with $\mathfrak{q} = 0$, i.e., for perturbations propagating just along the φ direction. The results obtained in this case are displayed in Fig. 3. The real part of the frequency is interpreted as the convective term, cf. Eq. (32). This term is positive when the perturbation wave vector has the same direction as the rotation velocity ($\mathfrak{m} > 0$), and is negative when the perturbation wave vector is in the opposite direction ($\mathfrak{m} < 0$). Both cases represent propagation in the direction of increasing φ, the same direction of the rotation velocity, as expected for a convection process. Following our choice of non-negative $\mathfrak{w}_R$, the graphs in Fig. 3 contain only the quasinormal frequencies for $\mathfrak{m} \geq 0$.

Furthermore, by comparing quantitatively the results of the imaginary parts for different values of the rotation parameter, e.g., $a\alpha = 0.1$ and $a\alpha = 1/\sqrt{2}$ (top and bottom panels in Fig. 3), we observe that $\mathfrak{w}_I^{a\alpha=0.1} > \mathfrak{w}_I^{a\alpha=0.71}$ (for a specific value of the wave number, e.g., $\mathfrak{m} = 1$). This means that the damping time for perturbations propagating on a black string with smaller rotation parameter are damped faster than the perturbations propagating on a black string with larger rotation parameter, i.e., $\tau^{a\alpha=0.1} < \tau^{a\alpha=0.71}$. Such a result is in agreement with the expected relativistic effect of time dilation. This kind of behavior has already been observed in a previous study of electromagnetic perturbations of rotating black strings [73].

C. Longitudinal sector—analytical results

The longitudinal sector (or sound channel) of the gravitational perturbations is governed by the differential equation (25). It is possible to solve this differential equation by using a perturbative expansion of Z_L in powers of $\mathfrak{w}$, $\mathfrak{m}$ and $\mathfrak{q}$, as it was originally done in Refs. [41,42]. However, here we use the relations between the frequencies and wave numbers of the static and rotating black strings, given by Eq. (19), and the dispersion relation for the static black string, as obtained in Refs. [44,70], namely,

$$\bar{\mathfrak{w}} = \pm\frac{1}{\sqrt{2}}\sqrt{\bar{\mathfrak{q}}^2 + \alpha^2\bar{\mathfrak{m}}^2} - \frac{i}{6}(\bar{\mathfrak{q}}^2 + \alpha^2\bar{\mathfrak{m}}^2) + \cdots. \quad (34)$$

First we note that the general dispersion relation for the longitudinal momentum fluctuations of a fluid is given by the sound wave mode

$$\bar{\omega} = \pm\bar{c}\sqrt{\bar{q}^2 + \alpha^2\bar{m}^2} - i\bar{\Gamma}(\bar{q}^2 + \alpha^2\bar{m}^2) + \cdots, \quad (35)$$

where $\bar{c}$ is the (phase) speed of sound and $\bar{\Gamma}$ is the sound wave damping constant. By comparing Eqs. (34) and (35), the phase speed and the damping constant are identified, respectively, by $\bar{c} = 1/\sqrt{2}$ and $\bar{\Gamma} = 1/(8\pi\mathcal{T})$. As in the transverse sector, the damping time is given by the inverse of the imaginary part, i.e., $\bar{\tau} = 1/\bar{\omega}_I$.

Therefore, by replacing relations (19) into Eq. (34) and following the same procedure as in the case of the transverse sector, specifically considering the expansion (31), we obtain

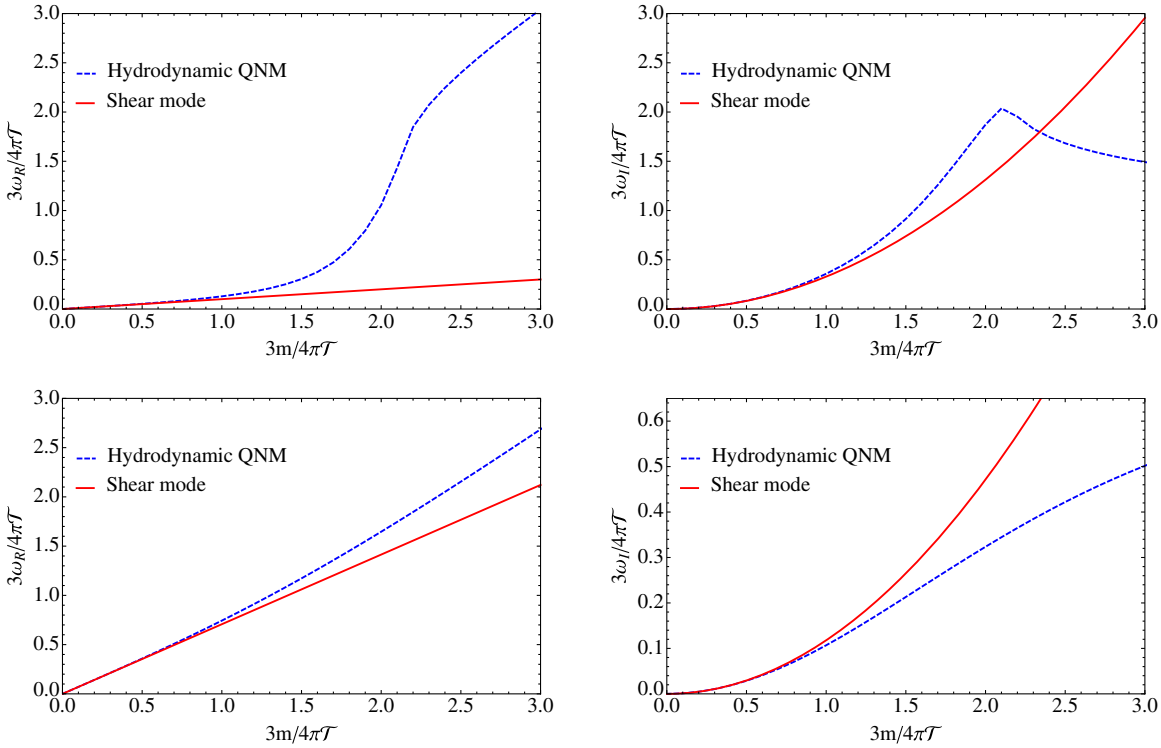

FIG. 3. Dispersion relations of the hydrodynamic QNMs (solid lines), cf. Eq. (32), and shear mode (dashed lines) of the transverse sector, with $\mathfrak{q}=0$, for $a\alpha=0.1$ (top panels) and $a\alpha=1/\sqrt{2}$ (bottom panels).

$$\mathfrak{w}=\frac{a\alpha\gamma^2}{1+\gamma^2}\alpha\mathfrak{m}\pm\frac{1}{1+\gamma^2}\sqrt{2\alpha^2\mathfrak{m}^2+(1+\gamma^2)\mathfrak{q}^2}-\frac{2i\gamma^3}{3(1+\gamma^2)^2}\mathfrak{q}^2-\frac{2i\gamma^3}{(1+\gamma^2)^3}\left(\frac{2}{3}+a^2\alpha^2\right)\alpha^2\mathfrak{m}^2\pm\frac{ia\alpha\gamma^3(6+a^2\alpha^2)}{3(1+\gamma^2)^3}\alpha\mathfrak{m}\sqrt{2\alpha^2\mathfrak{m}^2+(1+\gamma^2)\mathfrak{q}^2}\mp\frac{ia^3\alpha^3\gamma^3}{(1+\gamma^2)^2}\frac{\alpha\mathfrak{m}\mathfrak{q}^2}{\sqrt{2\alpha^2\mathfrak{m}^2+(1+\gamma^2)\mathfrak{q}^2}}+\cdots. \tag{36}$$

In order to interpret this result, we rewrite it in a more compact form. To do that, we introduce a new parameter c, defined by

$$c=\frac{(1-\bar{c}^2)a\alpha\cos\theta}{1-a^2\alpha^2\bar{c}^2}\pm\frac{\bar{c}\sqrt{1-a^2\alpha^2}}{1-a^2\alpha^2\bar{c}^2}\times\sqrt{1-a^2\alpha^2\bar{c}^2-(1-\bar{c}^2)a^2\alpha^2\cos^2\theta}, \tag{37}$$

where $\cos\theta=\mathfrak{m}\alpha/(\mathfrak{m}^2\alpha^2+\mathfrak{q}^2)^{1/2}$. In the dual CFT description, the modulus of the parameter c can be interpreted as the "speed of sound" in the cylinder rest frame K (the rotating black-string frame in the bulk). Differently from the value of the speed of sound $\bar{c}=1/\sqrt{2}$ in the fluid rest frame $\bar{K}$ (the static black-string frame) that is positive, by definition, c may be positive, zero or negative, depending on the propagation direction, because $\mathfrak{m}$ may assume all values in the real line (see, for instance, Fig. 5).

By writing Eq. (36) in terms of the parameter c and reintroducing the original quantities ω, q, and m from Eq. (18), it gives (see also Appendix for more details)

$$\omega=c\sqrt{m^2\alpha^2+q^2}-\frac{i}{8\pi\mathcal{T}\gamma(1-a\alpha\bar{c}\cos\bar{\theta})}\times\left[\gamma^2\left(1-\frac{a\alpha c}{\cos\theta}\right)^2m^2\alpha^2+q^2\right], \tag{38}$$

where $\cos\bar{\theta}=\bar{m}\alpha/(\bar{m}^2\alpha^2+\bar{q}^2)^{1/2}$.

Differently from the transverse sector, here it is not straightforward to identify the relativistic effects as the Lorentz contraction and the time dilation. By comparing, term by term, Eqs. (34) and (38), we can identify the generalized effects of time dilation and wavelength contraction in a situation where the wave is moving in both reference frames,

$$\tau=\gamma(1-a\alpha\bar{c}\cos\bar{\theta})\bar{\tau},\qquad\bar{m}\alpha=\gamma\left(1-\frac{a\alpha c}{\cos\theta}\right)m\alpha. \tag{39}$$

To simplify the analysis we consider some particular cases. By setting $\bar{\theta}=0$, $a\alpha=\bar{c}$, and by choosing the minus

sign solution from Eq. (37), we obtain the usual time dilation between the damping times, $\bar{\tau} = \gamma\tau$. Notice that, in this case, the frame K is comoving with the plane wave. Besides, the relation between the wave number components parallel to the rotation ($\bar{\theta} = 0 \Rightarrow \theta = 0$) reduces to $\bar{m} = \gamma m$ or, in terms of the wavelengths, $(2\pi/\bar{m}\alpha) = \gamma^{-1}(2\pi/m\alpha)$ (see also Appendix).

D. Longitudinal sector—numerical results

In this subsection we show the numerical solutions of the differential equation (25) for the lowest lying mode and compare the results to the analytical solutions (36). The results are displayed in Figs. 4 and 5, where the dashed lines represent the numerical results while solid lines represent the analytical solutions, respectively. As it was done for the transverse sector, to simplify the analysis and trying to get a clear physical interpretation of the results, the analysis is split into two cases.

First, we consider perturbations propagating perpendicularly to the rotation direction ($\mathfrak{m} = 0$). The results for this case are displayed in Fig. 4, where we observe that the real part of the frequency is proportional to $\mathfrak{q}$ in the hydrodynamic limit. From Eq. (36) we realize that the proportionality factor depends on the value of the rotation parameter and, to observe the effect of such a parameter, we plot three different cases: $a\alpha = 0.1$ (top panels), $a\alpha = 1/\sqrt{2} \approx 0.71$ (middle panels), and $a\alpha = 0.95$ (bottom panels). By comparing the real parts of the frequencies in this figure for a fixed value of the wave number, e.g., for $\mathfrak{q} = 1$, it is verified that when the rotation increases the real

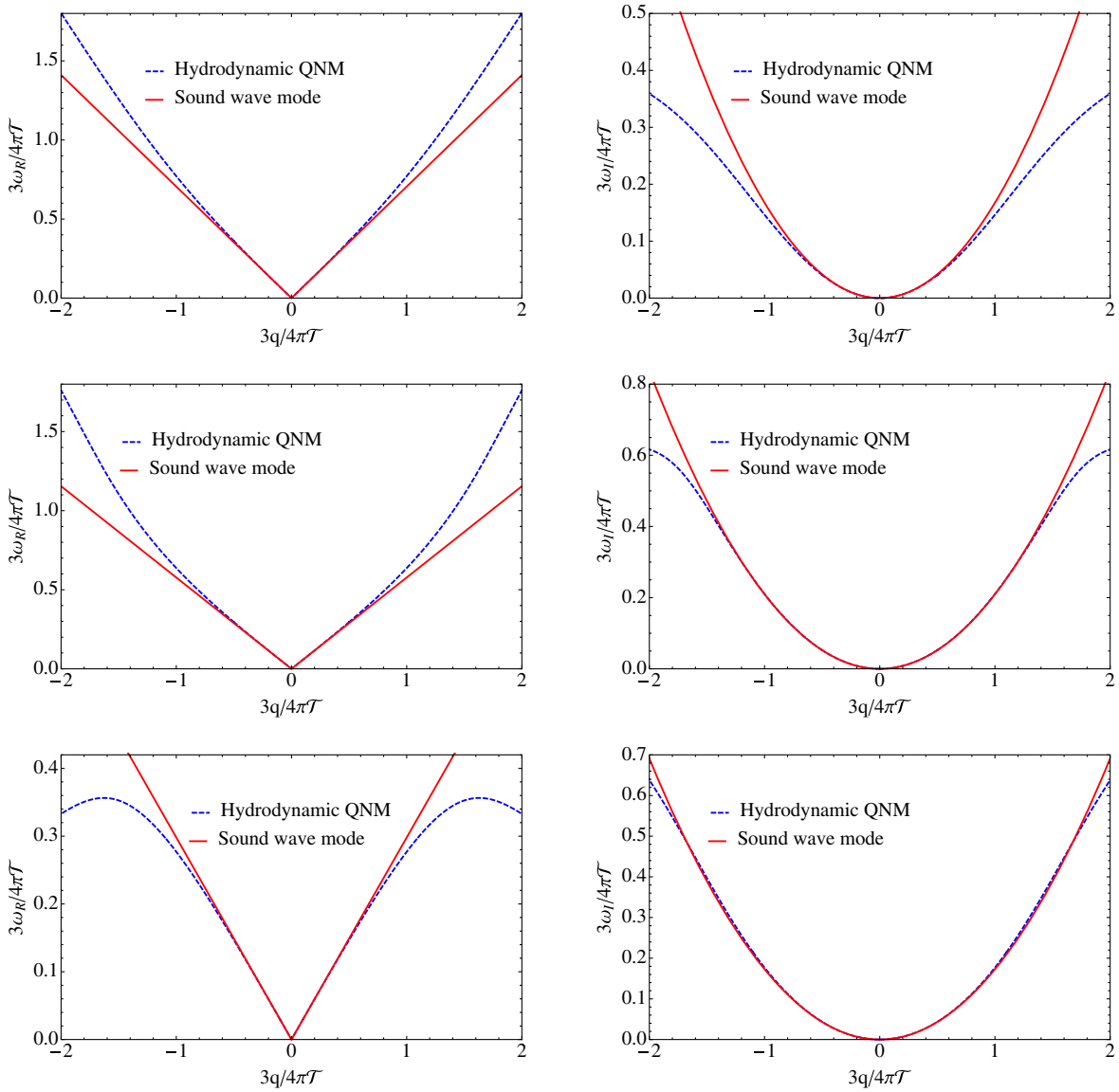

FIG. 4. Hydrodynamic QNMs (solid lines), cf. Eq. (36), and sound mode (dashed lines) of the longitudinal sector with $\mathfrak{m} = 0$ for $a\alpha = 0.1$ (top panels), $a\alpha = 1/\sqrt{2}$ (middle panels), and $a\alpha = 0.95$ (bottom panels).

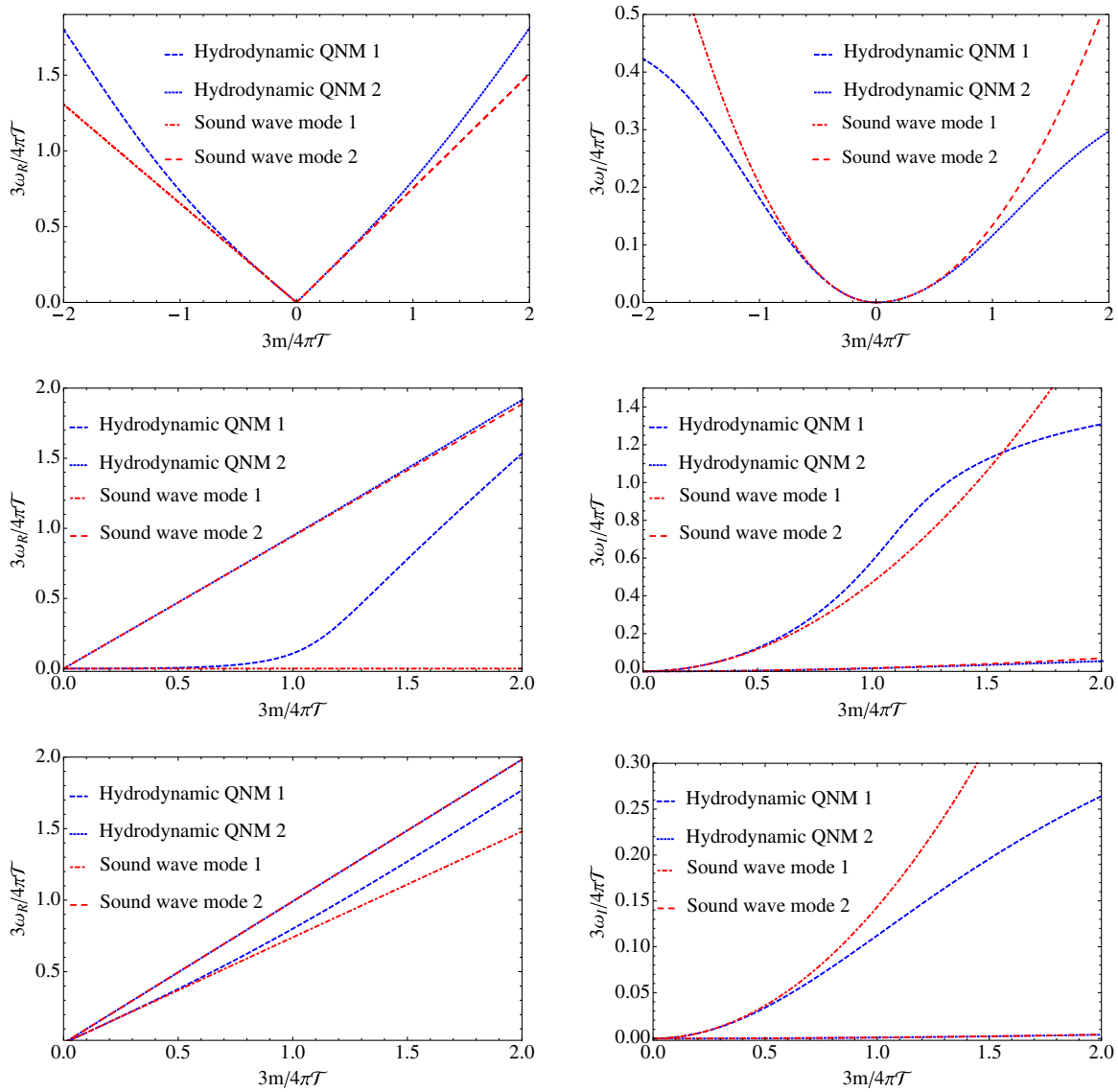

FIG. 5. Hydrodynamic QNMs (solid lines), cf. Eq. (36), and sound mode (dashed lines) of the longitudinal sector with $\mathfrak{q} = 0$ for $a\alpha = 0.1$ (top panels), $a\alpha = 1/\sqrt{2}$ (middle panels), and $a\alpha = 0.95$ (bottom panels).

part of the frequency decreases, i.e., $\mathfrak{w}_R^{a\alpha=0.1} > \mathfrak{w}_R^{a\alpha=0.71} > \mathfrak{w}_R^{a\alpha=0.95}$. This behavior is understood by noticing that, in the hydrodynamic approximation, given by Eq. (36), the leading term of the real part of the frequency is $\mathfrak{w}_R = \mathfrak{q}/\sqrt{1+\gamma^2}$, which decreases when $a\alpha$ increases.

On the other hand, the imaginary part of the frequency is proportional to q^2, and the corresponding coefficient,

$$\Gamma = \frac{\gamma^3}{2\pi\mathcal{T}(1+\gamma^2)^2}, \tag{40}$$

is associated to the damping of sound waves in the dual field theory. It is observed that the imaginary part of the frequency increases with the rotation parameter, as can be seen in the top and middle panels of Fig. 4, since $\mathfrak{w}_I^{a\alpha=0.1} < \mathfrak{w}_I^{a\alpha=0.71}$. This behavior remains until the rotation parameter reaches the critical value $(a\alpha)_c = \sqrt{2/3}$, where the sound wave damping coefficient attains a maximum value, decreasing from then on ($\mathfrak{w}_I^{a\alpha=0.71} > \mathfrak{w}_I^{a\alpha=0.95}$). This means that perturbations with the same wave numbers decay faster for higher rotation parameters if $a\alpha < (a\alpha)_c$, but decay more slowly if $a\alpha > (a\alpha)_c$. It is interesting to note that in the extremely rotating case, for $a\alpha = 1$, the damping coefficient vanishes, eliminating the imaginary part of the frequency, such that the QNMs become normal modes.

Second, we consider the case $\mathfrak{q} = 0$, which turns out to be a more interesting situation, cf. Fig. 5. In this case, the hydrodynamic approximation to the real part of the frequency is linear in $\mathfrak{m}$, with the proportionality

coefficient being the transformation of the velocity $\bar{c}$ to the moving frame, see Appendix for more details. Figure 5 displays three cases: $a\alpha = 0.1$ (top panels), $a\alpha = 1/\sqrt{2}$ (middle panels), and $a\alpha = 0.95$ (bottom panels). The graphs in all cases show good agreement between the analytical and the numerical results in the hydrodynamic limit. The deviation of the numerical results from the sound wave mode is also observed. Such deviation is easily understood by noticing that the analytical solutions are no longer valid beyond the hydrodynamic regime.

According to our conventions, assuming positive $\mathfrak{w}_R$, the perturbations with positive $\mathfrak{m}$ propagate in the same direction as the rotation, while the perturbations with a negative $\mathfrak{m}$ value propagate in the opposite direction. In the former case the real part of the frequency, obtained from the positive solution of Eq. (36), reduces to $[(\bar{c} + a\alpha)/(1 + a\alpha\bar{c})]\mathfrak{m}\alpha$, while in the opposite direction it becomes $[(\bar{c} - a\alpha)/(1 - a\alpha\bar{c})]\mathfrak{m}\alpha$. With these simplifications on hand we analyze in the following some interesting situations.

An interesting situation appears when the value of the rotation parameter equals the value of the speed of sound in the rest frame of the fluid, i.e., $a\alpha = \bar{c} = 1/\sqrt{2}$. The results for this situation are presented in the middle panels of Fig. 5. In this case, there are two hydrodynamic quasinormal modes for positive values of $\mathfrak{m}$, indicated respectively by QNM 1 and QNM 2, and none for negative values of $\mathfrak{m}$ with $\mathfrak{w}_R > 0$. The QNM 1 can be understood from Eq. (36). For negative $\mathfrak{m}$ and $a > 1/\sqrt{2}$ such equation furnishes frequencies with negative real part, representing in fact waves (positive frequencies) travelling along $+\varphi$ (with positive $\mathfrak{m}$, and hence these modes, like QNM 1, are plotted in the first quadrant of Fig. 5. Furthermore, by using the transformations (39), it is seen that the QNM 1 and QNM 2 correspond, respectively, to waves propagating in the $-\bar{\varphi}$ and $+\bar{\varphi}$ direction in the frame $\bar{K}$. For small wave number values, the real part of the QNM 1 frequency is essentially zero (within our numerical precision), while the real part of the QNM 2 frequency is $\mathfrak{w}_R \approx 2/\sqrt{2}$. Also, the QNM 1 frequency has relatively large imaginary part (in comparison to QNM 2), implying a small damping time $(1/\omega_I)$. Contrarily, the damping time of the hydrodynamic QNM 2 is large (in comparison to QNM 1), which means that the dissipative effects can be neglected in this case. Once the QNM 1 frequency has real part close to zero, it looks like a diffusion problem in the hydrodynamic regime. Such a result is expected in advance, since in this situation the frame K is comoving with the sound wave.

Bottom panels of Fig. 5 show the results for the case $a\alpha = 0.95$. We observe again the existence of two hydrodynamic QNMs for a given $\mathfrak{m} > 0$, one of them being associated to a wave propagating along the $-\bar{\varphi}$ direction of the frame $\bar{K}$. This effect can be interpreted in analogy to the case of an observer moving away from a source of sound waves that is at rest in relation to the medium. In the present case, as the velocity of the observer K, i.e., the rotation velocity of the black string, is larger than the speed of sound in the medium $(1/\sqrt{2})$, the observer detects all the wave fronts moving away from him in the opposite direction. Additionally, the imaginary part of the QNM 2 is very small, indicating that this perturbation mode is weakly damped.

V. NONHYDRODYNAMIC QUASINORMAL MODES

In this section, we investigate the nonhydrodynamic QNMs of the transverse and longitudinal sectors for a few different values of the rotation parameter, namely, for $a\alpha = 0.1, 0.2, 1/\sqrt{2}$ and 0.8. The frequencies of the nonhydrodynamic (or ordinary) modes are obtained by solving numerically the differential equations (22) and (25) for specific values of the wave numbers $\mathfrak{m}$ and $\mathfrak{q}$. The main difference between the nonhydrodynamic and the hydrodynamic QNMs is the behavior in the small wave number limit, with the hydrodynamic frequencies going to zero, while the nonhydrodynamic frequencies tend to nonzero values. The ration between the imaginary parts of successive frequencies at zero wave numbers is used to rank in increasing order the different nonhydrodynamic QNMs. Since their damping time $\tau = 1/\omega_I$ is relatively short for small wave numbers, the nonhydrodynamic modes are the first to disappear in this regime. Moreover, numerical studies on the time evolution of the perturbations show that such modes dominate the initial response of the system, i.e., they are the most relevant modes at early times after the perturbation takes place (see Ref. [72] as an example). Several works in this direction were published in the last few years due to its interpretation and relevance in the dual field theory, and mainly to get more information about the quark-gluon plasma before the hydrodynamic regime [83–85].

A. Transverse sector

The nonhydrodynamic QNM frequencies of the transverse sector are found by solving numerically the differential equation (22). The results displayed here are for wave numbers in the intervals $\mathfrak{m} \in [-10, 10]$ and $\mathfrak{q} \in [0, 10]$. In Fig. 6 we show the frequencies of the first five transverse nonhydrodynamic QNMs obtained for $a\alpha = 0.1$. The first difference to note in comparison to the static case studied in Ref. [70] is that the frequencies are now asymmetric under the change $\mathfrak{m} \to -\mathfrak{m}$. This result for the real parts of the frequencies may be understood in terms of the difference in the Doppler shift produced by the rotation as the waves propagate in the $+\varphi$ or $-\varphi$ directions.

Another fact worthy to be noted is the interconnection between two different neighbor modes, as it can be observed in Fig. 6, where a lower lying mode grows and reaches the first upper lying mode. This effect occurs at

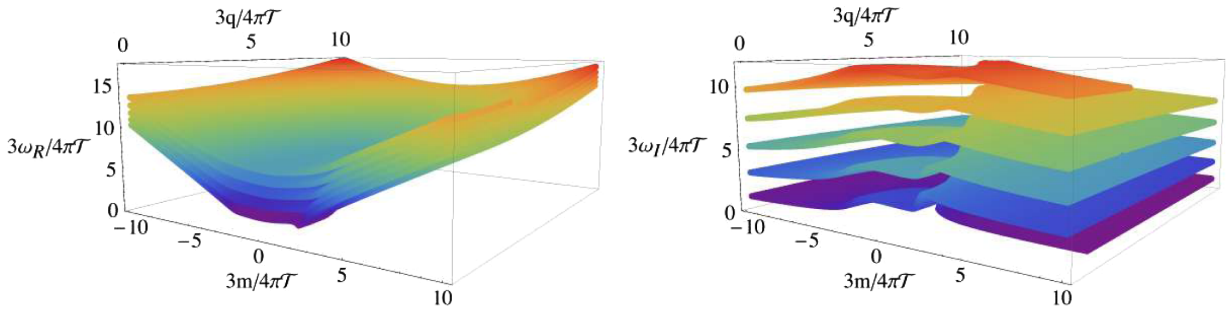

FIG. 6. The first five nonhydrodynamic modes of the transverse sector obtained by setting $a\alpha = 0.1$. The left (right) panel shows the real (imaginary) part of the frequency.

small $\mathfrak{q}$ and positive $\mathfrak{m}$ and is more evident for the imaginary parts of the frequencies. We still do not know the origin of such an effect that does not happen in the static black string case, and a physical interpretation for it is also missing.

To get more information from Fig. 6 we take two dimensional slices by choosing some fixed values of the wavenumber $\mathfrak{q}$. The slices for $\mathfrak{q} = 0$, 1, 2 and 3 of the first nonhydrodynamic mode are displayed in Fig. 7. As already mentioned, the asymmetry of the real (left panel) and imaginary (right panel) parts of the frequencies in relation to $\mathfrak{m}$ is a consequence of the rotation. The curves of $\mathfrak{w}_I$ against $\mathfrak{m}$ show the peculiar behavior observed in Fig. 6 for $\mathfrak{m} \gg 1$: the asymptotic behavior of the modes for small $\mathfrak{q}$ is very different from that for large $\mathfrak{q}$. Clearly there is a sharp jump at some intermediate value of $\mathfrak{q}$. However, in the $-\mathfrak{m}$ direction, the frequencies converge to the same value for all $\mathfrak{q}$.

On basis of Fig. 8 an additional analysis of the slice $\mathfrak{q} = 0$ is developed in the sequence. As mentioned above, we take the hydrodynamic QNM together with the first nonhydrodynamic mode because these are the dominant modes throughout the time evolution of the gravitational perturbations (see, for instance, Ref. [85]). In the top panels of Fig. 8 we display the absolute value of the QNM frequencies, $\mathfrak{w} = \sqrt{\mathfrak{w}_R^2 + \mathfrak{w}_I^2}$, as a function of the wave number component $\mathfrak{m}$ for $a\alpha = 0.1$ (top left panel) and $a\alpha = 1/\sqrt{2}$ (top right panel). In these graphics, it is possible to observe the different behaviors of the quasinormal frequencies in the low- and high-wave number regimes. To quantitatively measure these differences we calculate the slope of each curve through the relation

$$\partial_{\mathfrak{m}}\mathfrak{w} \equiv \frac{\partial \mathfrak{w}}{\partial \mathfrak{m}} \approx \frac{\Delta \mathfrak{w}}{\Delta \mathfrak{m}} = \frac{\mathfrak{w}_{i+1} - \mathfrak{w}_i}{\mathfrak{m}_{i+1} - \mathfrak{m}_i}. \tag{41}$$

Here $\mathfrak{w}_i$ and $\mathfrak{w}_{i+1}$ are numerical solutions calculated at neighbor wave number values $\mathfrak{m}_i$ and $\mathfrak{m}_{i+1}$, respectively. The bottom left panel in Fig. 8 shows the corresponding results for $a\alpha = 0.1$. In this figure we see a sharp jump close to the point $\mathfrak{m} \approx 2.1$ for both the hydrodynamic and the first nonhydrodynamic modes. A vertical line was plotted at this point. In the opposite direction, the hydrodynamic QNM still has this sharp jump at $\mathfrak{m} \approx -2.1$, while the nonhydrodynamic mode has a smooth transition. An important feature is that the dispersion relation of the nonhydrodynamic mode is approximately constant—the slope being approximately zero—between the two vertical lines. Asymptotically, for large wave numbers, the dispersion relations tend to be linear, which is characteristic behavior of the relativistic regime (see also Ref. [86]). Repeating the same analysis for $a\alpha = 1/\sqrt{2}$, we observe a

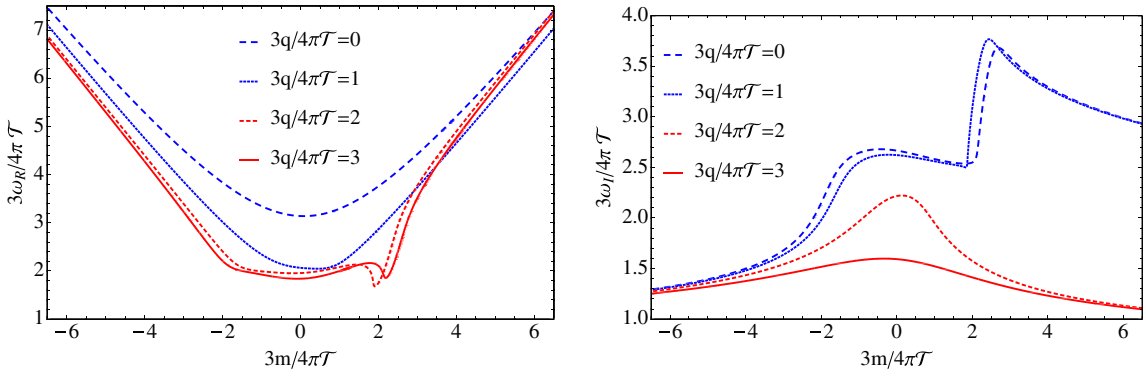

FIG. 7. The real (left panel) and imaginary (right panel) parts of the frequency of the first non-hydrodynamic QNM for different values of $\mathfrak{q} = 3q/4\pi\mathcal{T}$. This are two dimensional cuts of Fig. 6 at the given values of $\mathfrak{q}$.

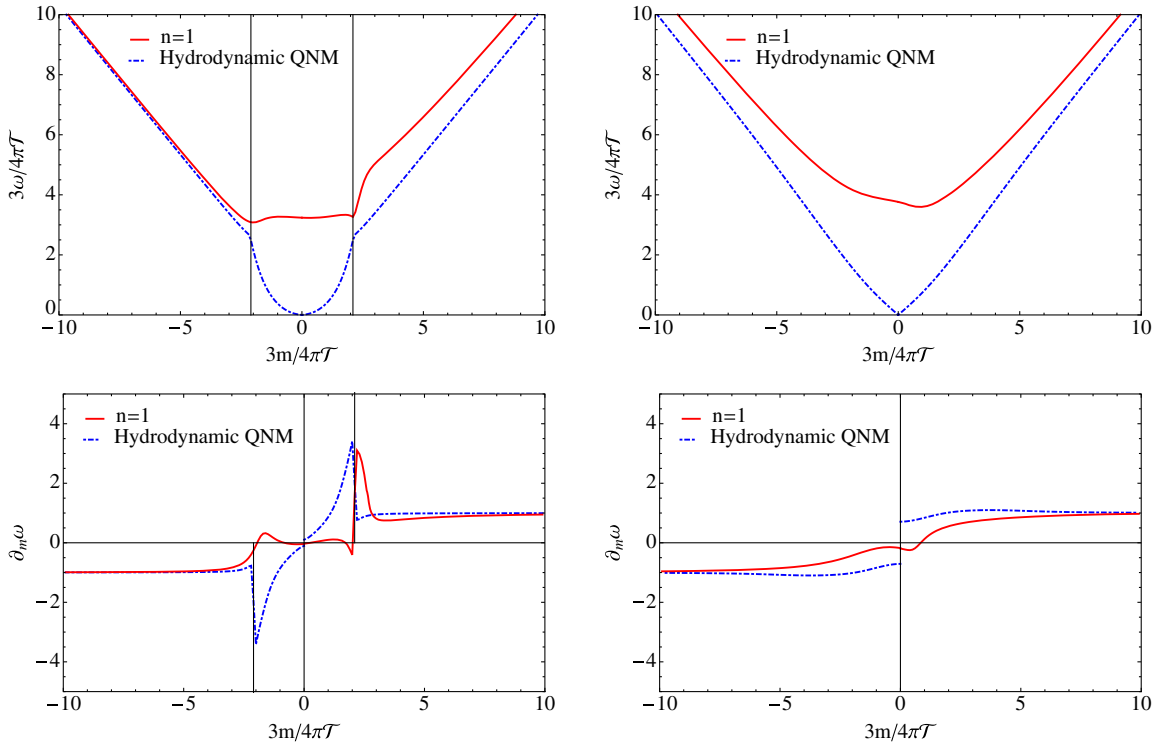

FIG. 8. The absolute values of the hydrodynamic and the first nonhydrodynamic QNMs of the transverse sector as a function of $\mathfrak{m}$ for $\mathfrak{q}=0$, with $a\alpha=0.1$ (top left panel), and $a\alpha=1/\sqrt{2}$ (top right panel). The bottom panels show the slope of the curves $\mathfrak{w}=\mathfrak{w}(\mathfrak{m})$, given by $\partial_{\mathfrak{m}}\mathfrak{w}$, for both cases shown in the top panels. The vertical lines in the left panels (top and bottom) are located at $\mathfrak{m}\approx 2.1$ and $\mathfrak{m}\approx -2.1$.

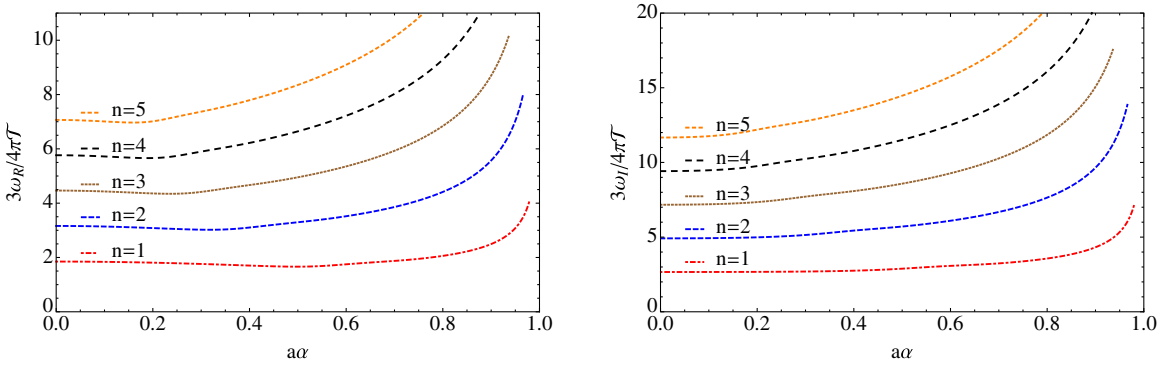

FIG. 9. The first five nonhydrodynamic QNMs of the transverse sector as a function of the rotation parameter for $\mathfrak{m}=\mathfrak{q}=0$.

smooth transition in the results displayed in the bottom right panel of Fig. 8.

The absolute values of the QNM frequencies, plotted in Fig. 8, exhibit two different regimes. This behavior is confirmed numerically by plotting the slope of the dispersion relations, given by $\partial_{\mathfrak{m}}\mathfrak{w}$, as shown in the bottom panels of Fig. 8. A sharp jump for $a\alpha=0.1$ and a smooth jump for $a\alpha=0.71$ are observed. Such a result might mean that there exists some kind of "phase transition" in the dual field theory: one phase dominated by a typical QNM behavior and another phase by a linear relativistic dispersion relation, as claimed in Ref. [86].

TABLE I. The first four nonhydrodynamic QNMs of the transverse sector for $a\alpha=0.2$, $a\alpha=1/\sqrt{2}$, and $a\alpha=0.8$, by setting $\mathfrak{q}=\mathfrak{m}=0$.

	$a\alpha=0.2$		$a\alpha=1/\sqrt{2}$		$a\alpha=0.8$	
n	$\mathfrak{w}_R$	$\mathfrak{w}_I$	$\mathfrak{w}_R$	$\mathfrak{w}_I$	$\mathfrak{w}_R$	$\mathfrak{w}_I$
1	1.80874	2.67375	1.88332	3.25760	2.05936	3.56685
2	3.08284	4.98585	3.88903	6.73601	4.41405	7.64535
3	4.35865	7.34553	5.98003	10.35772	6.84171	11.85020
4	5.66173	9.75472	8.09551	14.02184	9.28790	16.08711

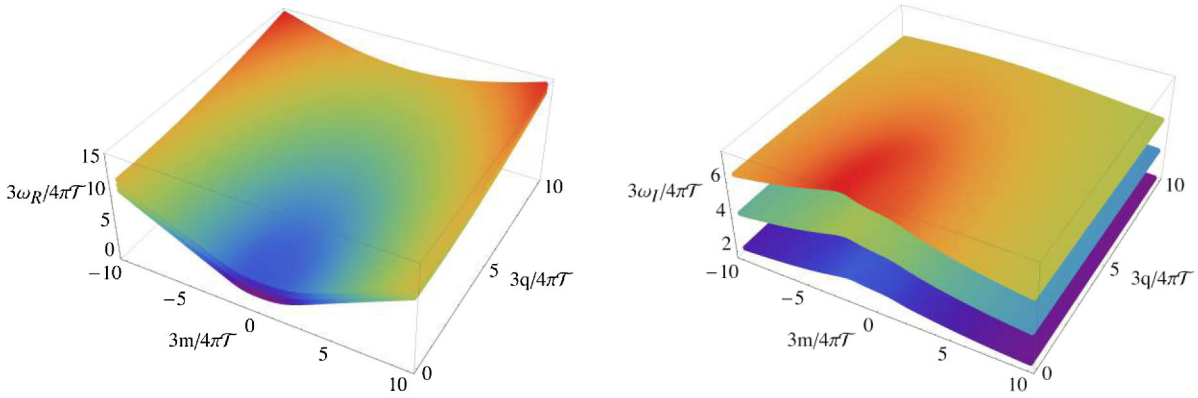

FIG. 10. The first three nonhydrodynamic modes of the longitudinal sector of perturbations. The left (right) panel shows the real (imaginary) part of the frequency. These results were obtained by setting $a\alpha = 0.1$.

Figure 8 also shows another important consequence of the rotation. In the case of $a\alpha = 0.1$ a transition from the hydrodynamic-like to the relativistic behavior is observed, an effect that was previously reported in Ref. [86] for the QNMs of electromagnetic perturbations. As the rotation parameter increases to $a\alpha = 1/\sqrt{2}$, such a transition is no longer evident. In the extremely rotating case, $a\alpha = 1$, the dispersion relation becomes linear, meaning that the relativistic behavior is dominant and no transition is observed.

To finish the analysis of the transverse-sector, in Fig. 9 we display the evolution of the first five non-hydrodynamic QNMs as a function of the rotation parameter $a\alpha$. For simplicity we choose $\mathfrak{m} = 0 = \mathfrak{q}$. These zero-wave number modes are interpreted as gravitational waves propagating in the radial direction. Additional information on the behavior of these modes in terms of the rotation parameter can be seen in Table I, where we write the frequencies of the first four non-hydrodynamic modes for some selected values of the rotation parameter. It is clearly seen that the frequency grows with $a\alpha$.

B. Longitudinal sector

The nonhydrodynamic QNM frequencies of the longitudinal sector are obtained by solving numerically the differential equation (25). Here we solve this equation for wave number values in the intervals $\mathfrak{m} \in [-10, 10]$ and $\mathfrak{q} \in [0, 10]$. We display the numerical results of the first three nonhydrodynamic modes in Fig. 10 for $a\alpha = 0.1$. As reported in Ref. [70], the real and imaginary parts of the frequencies of the static black string are symmetric under the changes $\mathfrak{m} \to -\mathfrak{m}$ and $\mathfrak{q} \to -\mathfrak{q}$. Here, the results show that the symmetry $\mathfrak{m} \to -\mathfrak{m}$ is broken because the rotation introduces a preferred direction. The asymmetry in the real part of the frequency may be interpreted as a Doppler shift.

Differently from the transverse sector, cf. Fig. 6, no interconnections between adjacent modes were observed. In Table II we write selected values of the frequency of the first four nonhydrodynamic modes; to obtain these results we set $\mathfrak{m} = 0 = \mathfrak{q}$.

As it was done for the transverse sector, to get additional information of the numerical results we plot slices of the absolute value of the frequency as a function of $\mathfrak{m}$ for $\mathfrak{q} = 0$. In the left top panel of Fig. 11 we plot the hydrodynamic and the first nonhydrodynamic quasinormal frequencies for $a\alpha = 0.1$. We also calculate the slope of the curves by means of numerical approximations for $\partial_{\mathfrak{m}}\mathfrak{w}$. The results are displayed in the left bottom panel of Fig. 11. For a (non)hydrodynamic QNM, it is observed a smooth transition between a (non)hydrodynamic like behavior for small wave numbers to a linear relativistic behavior in the regime of large wave numbers.

The right top panel of Fig. 11 displays the results for $a\alpha = 1/\sqrt{2}$. This figure shows the hydrodynamic and the first nonhydrodynamic quasinormal modes along the φ direction. The slope $\partial_{\mathfrak{m}}\mathfrak{w}$ was also calculated and the result is displayed in the bottom right panel of that figure. The plot shows a smooth transition from the small to the large wave number regimes.

To complete the analysis of the longitudinal sector we show in Fig. 12 the evolution of the first five nonhydrodynamic QNMs as a function of the rotation parameter for $\mathfrak{m} = 0 = \mathfrak{q}$. The behavior of these modes with the rotation parameter is similar to the case of the transverse sector.

TABLE II. The first four nonhydrodynamic QNMs of the longitudinal sector with zero wave numbers ($\mathfrak{q} = \mathfrak{m} = 0$) for $a\alpha = 0.2$, $a\alpha = 1/\sqrt{2}$, and $a\alpha = 0.8$.

	$a\alpha = 0.2$		$a\alpha = 1/\sqrt{2}$		$a\alpha = 0.8$	
n	$\mathfrak{w}_R$	$\mathfrak{w}_I$	$\mathfrak{w}_R$	$\mathfrak{w}_I$	$\mathfrak{w}_R$	$\mathfrak{w}_I$
1	1.80350	2.66783	1.24011	2.17621	1.16478	2.01591
2	3.05672	4.94665	2.89498	5.01419	3.22866	5.59221
3	4.28620	7.22177	4.93568	8.54886	5.62604	9.74459
4	5.50904	9.47953	7.03808	12.19031	8.06416	13.96753

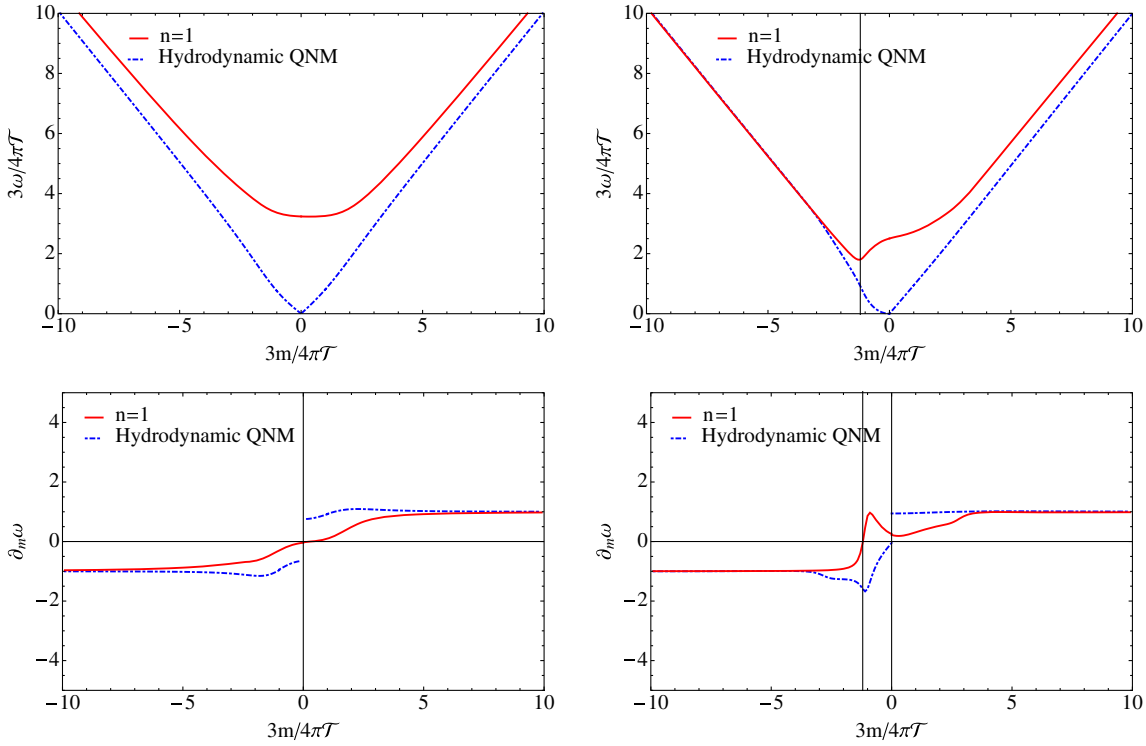

FIG. 11. The top panels show the absolute value of the frequency, $\mathfrak{w} = \sqrt{\mathfrak{w}_R^2 + \mathfrak{w}_I^2}$, for the hydrodynamic and the first non-hydrodynamic QNMs of the longitudinal sector as a function of $\mathfrak{m}$, with $\mathfrak{q} = 0$, and for two values of the rotation parameter: $a\alpha = 0.1$ (top left panel) and $a\alpha = 1/\sqrt{2}$ (top right panel). The bottom panels show the slope of the curves presented in the top panels. The right panels show a vertical line at $\mathfrak{m} = -1.2$.

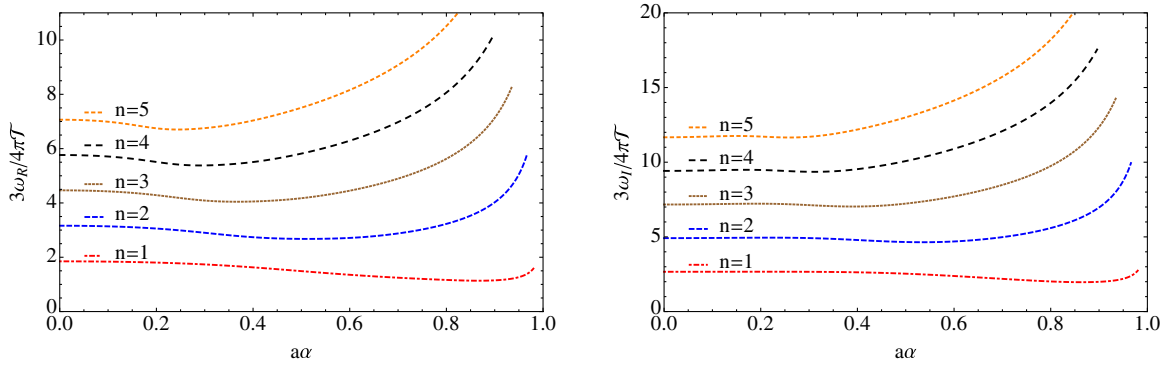

FIG. 12. The first five nonhydrodynamic QNMs of the longitudinal sector as a function of the rotation parameter for $\mathfrak{m} = \mathfrak{q} = 0$.

VI. EMERGENCE OF A NEW QNM CLASS AND THE ALGEBRAICALLY SPECIAL MODES

As commented previously, the QNMs of the rotating black strings are closely related to those of the static black strings. Therefore, for most of the modes, the dispersion relations of the static black string QNMs can be recovered from the dispersion relations of the rotating black string QNMs in the limit of $a\alpha \to 0$. However, during the search for non-hydrodynamic QNMs, new solutions arise in both sectors of the gravitational perturbations. These new frequencies do not have any similar in previous studies on static black strings (see, for instance, Refs. [68,70,72]), and arise when the numerical search for QNMs is performed close the imaginary axis. This is true, in particular, for zero wave numbers $\mathfrak{m} = 0 = \mathfrak{q}$. Figure 13 displays the evolution of the real and imaginary parts of the frequency of the transverse (top panel) and longitudinal (bottom panel) sectors, respectively, as a function of the wave number component $\mathfrak{m}$.

Another characteristic property of these modes is the behavior close to the static limit $a \to 0$. In order to see that we plot in Fig. 14 the first four QNMs of the transverse (left

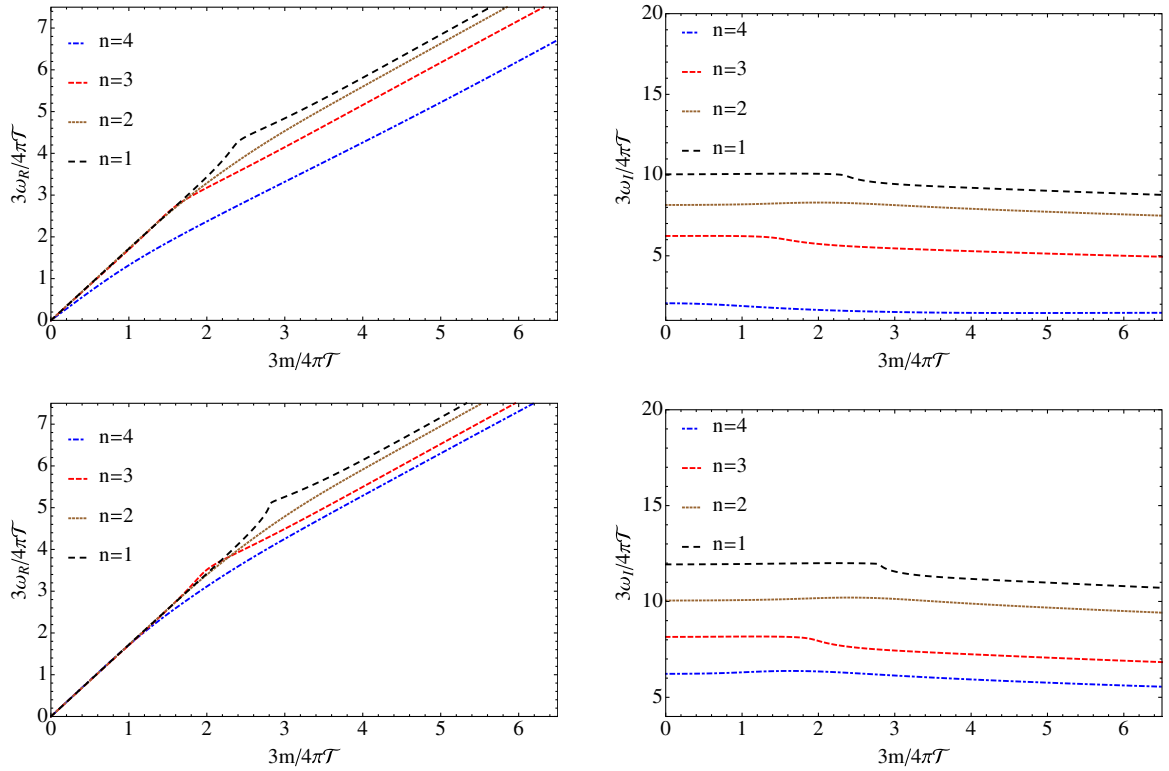

FIG. 13. First four modes that emerged in the transverse (top panel) and longitudinal (bottom panel) sector, as a function of the wave number $\mathfrak{m}$ for $\mathfrak{q} = 0$ and $a\alpha = 1/\sqrt{2}$.

panel) and longitudinal (right panel) sectors as a function of the rotation parameter. These frequencies raise to infinity when $a\alpha \to 0$, i.e., the value of the frequency diverges when the rotation parameter goes to zero. In fact, this is the reason why these modes are not found in the static black-string analysis. The numerical results indicate the existence of an infinite sequence of such modes.

It is worth mentioning at this point that it has appeared in the literature a few works studying purely damped modes of the Kerr black hole in asymptotically flat spacetimes [87,88]. They report on the appearance of frequencies that have the same behavior as presented in Fig. 14, but no physical interpretation was given for such perturbation modes. On the other hand, in the present case of rotating black strings in an asymptotically AdS background, the solutions have a clear physical interpretation, namely, they are gravitational quasinormal modes. In the holographic context, it was recently obtained a similar result in the study of perturbations of a five-dimensional 1-R charged black hole close to a critical point [89].

In complement to the previous analysis, we now explore a possible relationship between the modes of Fig. 14 and the algebraically special modes [90–92]. For the definition and more details on the algebraically special perturbations

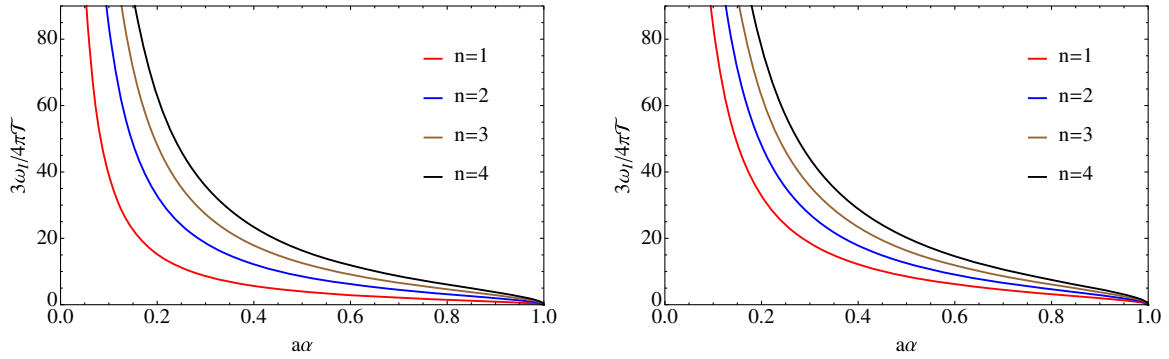

FIG. 14. The frequencies of the first fourth modes that emerged in the transverse (left panel) and longitudinal (right panel) sectors as a function of the rotation parameter for $\mathfrak{m} = \mathfrak{q} = 0$.

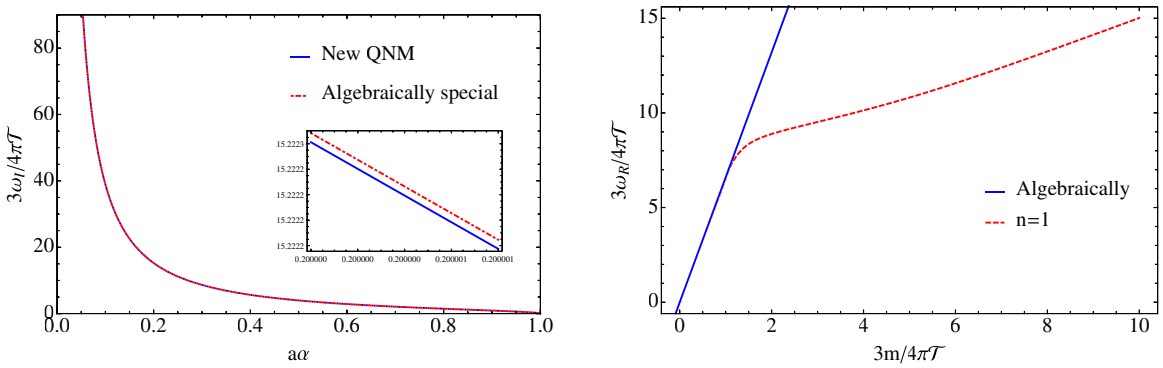

FIG. 15. Left panel: The algebraically special frequency (dashed line) and the first new quasinormal mode (solid line) as a function of the rotation parameter. Right panel: The dependence of the real parts of the frequencies of the first new purely damped mode (dashed line), and of the algebraically special mode (solid line) with the wave number value $\mathfrak{m}$. To get the results shown on the left panel we set $\mathfrak{m} = 0 = \mathfrak{q}$, while to get the results on right panel we set $\mathfrak{q} = 0$ and $a\alpha = 0.2$.

in the Kerr and Schwarzschild black holes see, e.g., [93–97]. It is verified numerically that the first ($n = 1$) QNM frequency of the transverse sector (left panel in Fig. 14) approaches one of the algebraically special frequencies in the limit of small values of the rotation parameter. This is shown in the left panel of Fig. 15. In order to verify such a relationship, we start reviewing the dispersion relation of an algebraically special mode. As found in previous works [70], static black strings possess an algebraically special frequency given by

$$\bar{\mathfrak{w}} = -\frac{i}{6}(\bar{\mathfrak{q}}^2 + \bar{\mathfrak{m}}^2\alpha^2)^2. \tag{42}$$

Hence, by replacing relations Eq. (19) into Eq. (42) we get some of the algebraically special frequencies of the rotating black strings. Such frequencies now have nontrivial dispersion relations

$$\gamma\mathfrak{w} = -i\frac{\gamma^4\alpha^4(\mathfrak{m} - a\mathfrak{w})^4}{6}, \tag{43}$$

where to simplify the analysis we have set $\mathfrak{q} = 0$. Solving Eq. (43) for $\mathfrak{w}$ and expanding the solutions around $\mathfrak{m} = 0$, we get

$$\mathfrak{w}_1^a = \frac{6^{1/3}e^{i5\pi/6}}{(a\alpha)^{4/3}\gamma} + \left(\frac{4}{3a\alpha} - \frac{a\alpha}{3}\right)\mathfrak{m}\alpha + \frac{2^{2/3}e^{i\pi/6}}{3^{7/3}(a\alpha)^{2/3}\gamma^3}(\mathfrak{m}\alpha)^2 + \cdots, \tag{44}$$

$$\mathfrak{w}_2^a = -\frac{6^{1/3}e^{i\pi/2}}{(a\alpha)^{4/3}\gamma} + \left(\frac{4}{3a\alpha} - \frac{a\alpha}{3}\right)\mathfrak{m}\alpha - \frac{2^{2/3}e^{i\pi/2}}{3^{7/3}(a\alpha)^{2/3}}(\mathfrak{m}\alpha)^2 + \cdots, \tag{45}$$

$$\mathfrak{w}_3^a = a\alpha(\mathfrak{m}\alpha) - \frac{e^{i\pi/2}}{6\gamma^5}(\mathfrak{m}\alpha)^4 + \cdots, \tag{46}$$

$$\mathfrak{w}_4^a = \frac{6^{1/3}e^{i\pi/6}}{(a\alpha)^{4/3}\gamma} + \left(\frac{4}{3a\alpha} - \frac{a\alpha}{3}\right)\mathfrak{m}\alpha + \frac{2^{2/3}e^{i5\pi/6}}{3^{7/3}(a\alpha)^{2/3}\gamma^3}(\mathfrak{m}\alpha)^2 + \cdots, \tag{47}$$

where the ellipses stand for higher order corrections and the superscript a refers to the algebraically special frequencies. From these results we observe the existence of nonvanishing real and imaginary parts of the frequencies $\mathfrak{w}_i^a (i = 1, \ldots, 4)$, contrary to the static case, where the algebraically special frequencies are purely imaginary numbers. We discard the solutions $\mathfrak{w}_1^a$ and $\mathfrak{w}_4^a$ because they have negative imaginary parts, representing unstable modes. We also discard $\mathfrak{w}_3^a$ because it does not present the same behavior of the modes of Fig. 14, whose frequencies are large for small rotation parameters. The remaining solution, $\mathfrak{w}_2^a$, assumes large values for small rotation parameters and the imaginary part is positive. It is worth noticing that this solution becomes purely damped when the wave number $\mathfrak{m}$ is zero. This particular solution is important because it coalesces into the first purely damped transverse QNM in the limit of zero angular momentum, $a\alpha \to 0$. In fact, this singular behavior was our guide to try to connect the new-class frequencies to the algebraically special frequencies. We realize that the first new transverse-sector quasinormal mode is very close to the algebraically special mode for small values of the rotation parameter, deviating from it as the rotation parameter increases. Quantitatively the difference between these two frequencies can be seen in Table III. These results are also shown in the left panel of Fig. 15.

Here we highlight the existence of an algebraically special mode of frequency (42) associated to the longitudinal perturbations. However, such a mode does not appear in the QNM spectrum of the longitudinal (polar) perturbations of a static black string [67,68]. Hence, as it could be expected, it was not found a connection between

TABLE III. The imaginary parts of the frequencies of the new-class transverse-sector QNMs and the algebraically special modes with $\mathfrak{q} = \mathfrak{m} = 0$.

$a\alpha$	$\mathfrak{w}_1$ (new mode)	$\mathfrak{w}_2^a$ (algebraic mode)
0.1	38.95244	38.95244
0.3	8.63127	8.63130
0.5	3.97043	3.96541
0.7	2.10127	2.08788
0.9	1.03380	0.91153
0.999	0.09796	0.08135

the frequencies (44)–(47) and the new-class QNMs of the longitudinal perturbations.

At this point one could ask if there exists a relation between the algebraically special frequencies, $\mathfrak{w}_2^a$, and the new family of QNMs for nonvanishing values of $\mathfrak{m}$ (or $\mathfrak{q}$). In order to answer such a question, we plot in Fig. 15 the joint results of the real part of the frequency of the algebraically special mode and the first new-class mode (right panel) as a function of the wave number component $\mathfrak{m}$. For small wave number values, the slope of the dispersion relation curve is precisely the coefficient of the real part of the frequency in Eq. (45), and it is the same for both frequencies. This is true at least for values of the rotation parameter smaller than $a\alpha = 0.5$. Doing the same analysis for several values of the rotation parameter (we do not present the whole results here), we arrive at the conclusion that, at least for the first new mode, the modes are numerically indistinguishable. Contrary to what happens in the static case, where the hydrodynamic QNM approaches asymptotically to the algebraically special frequency for large wave number values, here the opposite situation is verified. The first new QNM, $n = 1$, approaches to the algebraically special frequency as the rotation parameter decreases, cf. Fig. 14. We also realize that the evolution of the first new QNM frequency as a function of the wave number is approximately the same as the algebraically special frequency for small values of the wave number, as it can be seen in the right panel of Fig. 15.

We cannot say much about the new modes in the longitudinal sector because, in this case, we do not have an analytical expression for the static black string as the algebraically special frequency (42). However, the behavior of the new QNMs of the longitudinal perturbations seems to be similar to those of the transverse-sector QNMs.

VII. FINAL COMMENTS AND CONCLUSION

We developed a detailed analysis of the gravitational quasinormal modes of rotating black strings. First we explored the relation between the Regge-Wheeler-Zerilli (RWZ) and Kovtun-Starinets (KS) gauge-invariant quantities to get the equations of motion in the KS variables. After that, we obtained solutions of the differential equations for the hydrodynamic quasinormal modes through analytic and numeric methods. The analytic solutions show the corrections in the dispersion relations due to rotation. An example is the appearance of a nonzero term associated to convection in the real part of the shear mode frequency. On the other hand, the sound wave mode has an intricate dispersion relation due to the mixture of relativistic effects like the Lorentz contraction, the time dilation, and the transformation of the sound velocity, which become evident by considering some particular cases, cf. for instance, Figs. 3 and 5. In both sectors, the Doppler effect appears in our results as a consequence of the finite angular momentum of the black string.

The nonhydrodynamic QNMs were investigated by means of numerical methods. We found that the transverse sector exhibits an interconnection between successive modes, cf. Figs. 6 and 7. Additional information was obtained by calculating the absolute values of the frequencies, where it was observed a crossover from a (non) hydrodynamic like behavior to the linear relativistic scaling for small values of the rotation parameter, cf. the top left panel in Fig. 8. By increasing the value of the rotation parameter, the crossover is no longer observed, cf. top right panel in Fig. 8. This result is expected since for large values of the rotation parameter the system presents a typical relativistic behavior. The results for the longitudinal sector do not present an interconnection between successive modes.

Additionally, we have found a new class of quasinormal frequencies that does not have a similar counterpart in the QNM spectra of static black strings. These modes appear in both sectors and may be identified due to their peculiar dependence on the rotation parameter, cf. Fig. 14. In the transverse sector, the first mode of this new family of QNMs has a similar behavior as the algebraically special frequency, and approaches the last one in the limit of zero rotation parameter. We also have shown the evolution of the first new mode with the wave number, cf. the right panel of Fig. 15. It is worth mentioning also that these new frequencies are purely damped in the limit of zero wave numbers.

We finish this work by mentioning one of our outlooks concerning the present work. The immediate goal is to explore how the above results change when the electric charge is introduced in the rotating black strings. We may follow the study on gravitoelectromagnetic perturbations of rotating charged black strings of Ref. [80] for this purpose.

ACKNOWLEDGMENTS

We thank Alejandra Kandus, Alfonso Ballon-Bayona, Jorge Noronha and Saulo Diles for useful discussions and suggestions during the development of this work. V. T. Z. thanks financial support from Conselho Nacional de Desenvolvimento Científico e Tecnológico

(CNPq, Brazil), Grant No. 308346/2015-7, and from Coordenação de Aperfeiçoamento do Pessoal de Nível Superior (CAPES, Brazil), Grant No. 88881.064999/2014-01. L. A. H. M. thanks financial support from Fundação de Amparo à Pesquisa do Estado de São Paulo (FAPESP, Brazil), Grant No. 2013/17642-5, and from Coordenação de Aperfeiçoamento do Pessoal de Nível Superior - Programa Nacional de Pós-Doutorado (PNPD/CAPES, Brasil).

APPENDIX: RELATIVISTIC WAVE VECTORS

The main goal of this Appendix is to find the dispersion relations of sound waves propagating in a moving fluid from the known dispersion relations in the fluid rest frame. The motivation for this alternative analysis is to get a better understanding of the dispersion relations obtained in the study of the gravitational perturbations of rotating black strings, e.g., Eq. (36) of Sec. IV C. For that, we start reviewing the sound-wave propagation in a medium (which is identified as the CFT plasma in the AdS/CFT duality) and the wave vector transformation under a Lorentz boost.

Let $\bar{K}$ and K denote two inertial reference frames. Later on we shall identify $\bar{K}$ as the rest frame and K as the moving frame with respect to the fluid. The relations between the four-vector components $\bar{k}^\mu$ (defined in the frame $\bar{K}$) and k^μ (in the frame K) is $k^\mu = \Lambda^\mu{}_\nu \bar{k}^\nu$, where Λ^μ_ν is the Lorentz transformation matrix. In the present case, the fluid lives in a $(2+1)$-dimensional Minkowski spacetime. Explicitly, we may write (see, e.g., Ref. [98]):

$$\begin{cases} \omega = \gamma(\bar{\omega} - \boldsymbol{v}\cdot\bar{\boldsymbol{k}}), \\ k_\parallel = \gamma(\bar{k}_\parallel - v\bar{\omega}), \\ \boldsymbol{k}_\perp = \bar{\boldsymbol{k}}_\perp, \end{cases} \tag{A1}$$

where $\boldsymbol{v}$ is the velocity of frame $\bar{K}$ with respect to K, $\bar{k}_\parallel$ ($k_\parallel$) and $\bar{\boldsymbol{k}}_\perp$ ($\boldsymbol{k}_\perp$) are, respectively, the parallel and perpendicular components of the wave vector with respect to $\boldsymbol{v}$. In order to compare with the results presented in the previous sections, we identify $\boldsymbol{v} = \boldsymbol{a}\alpha$, where boldfaced symbols are used to indicate the spatial parts of vectors in the $(2+1)$-dimensional Minkowski spacetime. The form of Eq. (A1) guarantees the invariance of the phase of the plane waves. For a discussion on this point see, for instance, Ref. [99]. The angular frequency in the rest frame $\bar{K}$ is $\bar{\omega} = \bar{\boldsymbol{k}}\cdot\bar{\boldsymbol{u}}_p$, where $\bar{\boldsymbol{u}}_p$ is the phase velocity, with longitudinal projection given by $\bar{\boldsymbol{u}}_p^L = (\bar{\boldsymbol{k}}\cdot\bar{\boldsymbol{u}}_p)\bar{\boldsymbol{k}}/\bar{k}^2$. The transverse components of the phase velocity are indefinite [99]. Analogously, in the moving frame K, the angular frequency is $\omega = \boldsymbol{k}\cdot\boldsymbol{u}_p$. From here on, in this Appendix, we also use the relations $\bar{\omega} = \bar{\boldsymbol{k}}\cdot\bar{\boldsymbol{u}}_p = \bar{k}\,\bar{c}$ in frame $\bar{K}$, and $\omega = \boldsymbol{k}\cdot\boldsymbol{u}_p = kc$ in frame K.

Our next task is then to transform the identity $\bar{\omega} = \bar{c}\,\bar{k}$ from $\bar{K}$ to the new frame K, i.e., we are interested in obtained the transformed quantities ω, c, and k entering the identity $\omega = ck$ in frame K. By applying the inverse of Lorentz transformation (A1) to such an identity it follows

$$\gamma(\omega - vk_\parallel) = \bar{c}\,\sqrt{\gamma^2(k_\parallel - v\omega)^2 + \boldsymbol{k}_\perp^2}\,. \tag{A2}$$

To complete the transformation, it is necessary to find the transformation from the speed $\bar{c}$ in frame $\bar{K}$ to the speed c in the new frame K. We then solve Eq. (A2) for the frequency ω and use the identity $\omega = ck$ to get

$$c = \frac{(1-\bar{c}^2)v\cos\theta}{1-v^2\bar{c}^2} \pm \frac{\bar{c}\,\sqrt{1-v^2}\,\sqrt{1-v^2\bar{c}^2-(1-\bar{c}^2)v^2\cos^2\theta}}{1-v^2\bar{c}^2}, \tag{A3}$$

where we used the relations $k_\parallel = k\cos\theta$ and $|\boldsymbol{k}_\perp| = k\sin\theta$. A similar result to Eq. (A3) was found in the context of relativistic (super)fluids in Ref. [100].

Now we are ready to deal with the dispersion relations in both reference frames. We know the dispersion relation of a sound wave propagating in a dissipative medium in the rest frame of the fluid (see, for instance, Ref. [101]), as being

$$\bar{\omega} = \bar{c}\,\sqrt{\bar{k}_\parallel^2 + \bar{\boldsymbol{k}}_\perp^2} - \frac{i(\zeta+\eta)}{2(\epsilon+p)}(\bar{k}_\parallel^2 + \bar{\boldsymbol{k}}_\perp^2) + \mathcal{O}(\bar{k}^3, \bar{k}^4, \cdots). \tag{A4}$$

Quantities ζ, η, ϵ and p are, respectively, the bulk viscosity, shear viscosity, energy density and the pressure of the fluid. The additional terms, i.e., $\mathcal{O}(\bar{k}^3, \bar{k}^4, \cdots)$, are subleading terms in the regime where the frequency and wave number are of the same order. Here, it is interesting to point out that in a CFT fluid $\epsilon = 2p$ and $\zeta = 0$.

In order to build the dispersion relation in the frame K, we start with the expression of the invariant wave phase written in both frames [99],

$$\phi = \bar{\omega}\,\bar{t} - \bar{\boldsymbol{k}}\cdot\bar{\boldsymbol{r}} = \omega t - \boldsymbol{k}\cdot\boldsymbol{r}. \tag{A5}$$

Taking the derivative of Eq. (A5) with respect to time t, considering a constant phase and using Lorentz transformations, it follows

$$\omega = \boldsymbol{k}\cdot\boldsymbol{u}_p + \frac{1}{\gamma(1-\boldsymbol{v}\cdot\bar{\boldsymbol{u}}_p)}(\bar{\omega} - \bar{\boldsymbol{k}}\cdot\bar{\boldsymbol{u}}_p), \tag{A6}$$

where $\boldsymbol{u}_p = d\boldsymbol{r}/dt$ and $\bar{\boldsymbol{u}}_p = d\bar{\mathbf{r}}/d\bar{t}$ are the wave velocities, i.e., the phase velocities in each reference frame. Notice that, at first order approximation in the frequencies and wave numbers, Eq. (A6) is trivially satisfied. However, we

now are assuming that the dispersion relations are no longer linear. This means that the relation $\bar{\omega} = \bar{c}\,\bar{k}$ (or $\omega = ck$ in frame K) are first order approximations to the full dispersion relation.

Finally, the dispersion relation in the new frame can be obtained by substituting the relation $\boldsymbol{k}\cdot\boldsymbol{u}_p \equiv kc$ and Eq. (A4) into (A6),

$$\omega = c\sqrt{k_\parallel^2 + \boldsymbol{k}_\perp^2} - \frac{i(\zeta+\eta)}{2\gamma(\epsilon+p)(1-\boldsymbol{v}\cdot\bar{\boldsymbol{u}}_p)} \times\left[\gamma^2 k_\parallel^2\left(1-\frac{vc}{\cos\theta}\right)^2 + \boldsymbol{k}_\perp^2\right] + \cdots. \tag{A7}$$

Notice that $\boldsymbol{v}\cdot\bar{\boldsymbol{u}}_p = v\bar{c}\cos\bar{\theta}$, where $\cos\bar{\theta} = \bar{k}_\parallel/\bar{k}$. Equation (A7) is equivalent to Eq. (36) obtained in Sec. IV C. Here we prove this equivalence at least for the linear term in the wave numbers. We start by replacing Eq. (A3) into Eq. (A7) to get

$$\omega = \frac{(1-\bar{c}^2)vk_\parallel}{1-v^2\bar{c}^2} \pm \frac{\bar{c}\sqrt{1-v^2}}{1-v^2\bar{c}^2} \times\sqrt{(1-v^2\bar{c}^2)k^2 - (1-\bar{c}^2)v^2(k_\parallel)^2}, \tag{A8}$$

where it was taken into account the $\pm$ signs of Eq. (A3). Then, by setting $k_\parallel = k\cos\theta = \alpha m$, $k_\perp = k\sin\theta = q$, $\bar{c} = 1/\sqrt{2}$, $v = a\alpha$, and $(a\alpha)^2 = 1 - 1/\gamma^2$, after algebraic simplifications we obtain

$$\omega = \frac{a\alpha\gamma^2}{1+\gamma^2}\alpha m \pm \frac{1}{1+\gamma^2}\sqrt{2\alpha^2 m^2 + (1+\gamma^2)q^2}. \tag{A9}$$

Notice that the right-hand side of (A9) is precisely the linear term of Eq. (36). The proof of the equivalence for the higher order terms requires additional algebraic manipulations and we do not present here.

By comparing the results (A4) and (A7), we obtain a little more clarification about the imaginary part of the frequency. Setting $k_\perp = 0$ (to simplify the analysis) in Eq. (A7) and considering the $\pm$ signs in Eq. (A3) we obtain the relation

$$\omega_I = \frac{(1-v\bar{c})}{\gamma(1+v\bar{c})^2}\bar{\omega}_I \tag{A10}$$

for the plus sign, and

$$\omega_I = \frac{1}{\gamma(1-v\bar{c})}\bar{\omega}_I \tag{A11}$$

for the minus sign. In the last two relations, $\bar{\omega}_I$ is the imaginary part of the frequency in the fluid rest frame $\bar{K}$, namely,

$$\bar{\omega}_I = \frac{1}{2}\frac{\eta+\zeta}{\epsilon+p}\bar{k}_\parallel^2. \tag{A12}$$

The imaginary part of the frequency in the moving frame K, ω_I, is modified (contracted) by the Lorentz factor γ, and it is also modified due to the relative motion by the factors $(1-v\bar{c})$ and $(1+v\bar{c})$.

Taking into account that the damping time τ goes as the inverse of the imaginary part of the wave frequency, i.e., $.\tau = 1/\omega_I$, for (A10) it follows

$$\tau = \gamma^3\frac{(1+v\bar{c})^2}{(1-v\bar{c})}\bar{\tau}, \tag{A13}$$

while for (A11) it gives

$$\tau = \gamma(1-v\bar{c})\bar{\tau}, \tag{A14}$$

where $\bar{\tau}$ and τ are the damping times in the frames $\bar{K}$ and K, respectively. Equations (A13) and (A14) are valid for arbitrary values of the velocity v. By taking $v = \bar{c}$ into Eq. (A14), it becomes $\tau = \bar{\tau}/\gamma$ which is the time dilation effect.

Furthermore, yet by comparing Eqs. (A4) and (A7) we see that the parallel wave number component changes as follows

$$\bar{k}_\parallel = \left(1-\frac{vc}{\cos\theta}\right)\gamma k_\parallel. \tag{A15}$$

Considering the particular situation where $k_\perp = 0$ or, equivalently $\theta = 0$, the plus sign solution of Eq. (A3) can be written as $c = (v+\bar{c})/(1+v\bar{c})$. Replacing into Eq. (A15) it reduces to

$$k_\parallel = (1+v\bar{c})\gamma\bar{k}_\parallel. \tag{A16}$$

On the other hand, by considering the minus sign solution and taking $\theta = 0$ into Eq. (A3) it can be written as $c = (v-\bar{c})/(1-v\bar{c})$, so that Eq. (A15) reduces to

$$k_\parallel = (1-v\bar{c})\gamma\bar{k}_\parallel. \tag{A17}$$

Replacing $v = \bar{c}$ in Eq. (A17) it reduces to $k_\parallel = \bar{k}_\parallel/\gamma$ which is the Lorentz contraction. It is worth to point out that by doing $v = \bar{c}$ the observer K is comoving with the frame of the wave front.

[1] J. M. Maldacena, The large-N limit of superconformal field theories and supergravity, Int. J. Theor. Phys. **38**, 1113 (1999); Adv. Theor. Math. Phys. **2**, 231 (1998).

[2] E. Witten, Anti-de Sitter space and holography, Adv. Theor. Math. Phys. **2**, 253 (1998).

[3] S. S. Gubser, I. R. Klebanov, and A. M. Polyakov, Gauge theory correlators from non-critical string theory, Phys. Lett. B **428**, 105 (1998).

[4] O. Aharony, S. S. Gubser, J. M. Maldacena, H. Ooguri, and Y. Oz, Large N field theories, string theory and gravity, Phys. Rep. **323**, 183 (2000).

[5] J. Polchinski and M. J. Strassler, Hard Scattering and Gauge/String Duality, Phys. Rev. Lett. **88**, 031601 (2002).

[6] T. Sakai and S. Sugimoto, Low energy hadron physics in holographic QCD, Prog. Theor. Phys. **113**, 843 (2005).

[7] H. Boschi-Filho and N. R. F. Braga, Gauge/string duality and hadronic physics, Braz. J. Phys. **37**, 567 (2007).

[8] J. Erdmenger, N. Evans, I. Kirsch, and E. Threlfall, Mesons in gauge/gravity duals—A review, Eur. Phys. J. A **35**, 81 (2008).

[9] C. P. Herzog, Lectures on holographic superfluidity and superconductivity, J. Phys. A **42**, 343001 (2009).

[10] S. A. Hartnoll, Lectures on holographic methods for condensed matter physics, Classical Quantum Gravity **26**, 224002 (2009).

[11] J. McGreevy, Holographic duality with a view toward many-body physics, Adv. High Energy Phys. **2010**, 723105 (2010).

[12] M. Rangamani, Gravity and Hydrodynamics: Lectures on the fluid-gravity correspondence, Classical Quantum Gravity **26**, 224003 (2009).

[13] V. E. Hubeny and M. Rangamani, A Holographic view on physics out of equilibrium, Adv. High Energy Phys. **2010**, 297916 (2010).

[14] P. Kovtun, Lectures on hydrodynamic fluctuations in relativistic theories, J. Phys. A **45**, 473001 (2012).

[15] A. Karch, E. Katz, D. T. Son, and M. A. Stephanov, Linear confinement and AdS/QCD, Phys. Rev. D **74**, 015005 (2006).

[16] C. A. Ballon Bayona, H. Boschi-Filho, and N. R. F. Braga, Deep inelastic scattering from gauge string duality in D3-D7 brane model, J. High Energy Phys. 09 (2008) 114.

[17] A. S. Miranda, C. A. Ballon Bayona, H. Boschi-Filho, and N. R. F. Braga, Black-hole quasinormal modes and scalar glueballs in a finite-temperature AdS/QCD model, J. High Energy Phys. 11 (2009) 119.

[18] P. Colangelo, F. Giannuzzi, and S. Nicotri, Holographic approach to finite temperature QCD: The case of scalar glueballs and scalar mesons, Phys. Rev. D **80**, 094019 (2009).

[19] C. A. Ballon Bayona, H. Boschi-Filho, N. R. F. Braga, and M. A. C. Torres, Deep inelastic scattering for vector mesons in holographic D4-D8 model, J. High Energy Phys. 10 (2010) 055.

[20] P. Colangelo, F. Giannuzzi, and S. Nicotri, In-medium hadronic spectral functions through the soft-wall holographic model of QCD, J. High Energy Phys. 05 (2012) 076.

[21] L. A. H. Mamani, A. S. Miranda, H. Boschi-Filho, and N. R. F. Braga, Vector meson quasinormal modes in a finite-temperature AdS/QCD model, J. High Energy Phys. 03 (2014) 058.

[22] E. Folco Capossoli and H. Boschi-Filho, Deep inelastic scattering in the exponentially small Bjorken parameter regime from the holographic softwall model, Phys. Rev. D **92**, 126012 (2015).

[23] A. Ballon-Bayona, H. Boschi-Filho, L. A. H. Mamani, A. S. Miranda, and V. T. Zanchin, Effective holographic models for QCD: Glueball spectrum and trace anomaly, Phys. Rev. D **97**, 046001 (2018).

[24] S. S. Gubser, Breaking an Abelian gauge symmetry near a black hole horizon, Phys. Rev. D **78**, 065034 (2008).

[25] S. A. Hartnoll, C. P. Herzog, and G. T. Horowitz, Building a Holographic Superconductor, Phys. Rev. Lett. **101**, 031601 (2008).

[26] S. A. Hartnoll, C. P. Herzog, and G. T. Horowitz, Holographic superconductors, J. High Energy Phys. 12 (2008) 015.

[27] S. A. Hartnoll and P. Kovtun, Hall conductivity from dyonic black holes, Phys. Rev. D **76**, 066001 (2007).

[28] M. Blake and A. Donos, Quantum Critical Transport and the Hall Angle, Phys. Rev. Lett. **114**, 021601 (2015).

[29] J. Lindgren, I. Papadimitriou, A. Taliotis, and J. Vanhoof, Holographic Hall conductivities from dyonic backgrounds, J. High Energy Phys. 07 (2015) 094.

[30] O. Bergman, N. Jokela, G. Lifschytz, and M. Lippert, Quantum Hall Effect in a Holographic Model, J. High Energy Phys. 10 (2010) 063.

[31] A. Bayntun, C. P. Burgess, B. P. Dolan, and S. S. Lee, AdS/QHE: Towards a holographic description of quantum Hall experiments, New J. Phys. **13**, 035012 (2011).

[32] N. Jokela, M. Jarvinen, and M. Lippert, A holographic quantum Hall model at integer filling, J. High Energy Phys. 05 (2011) 101.

[33] S. S. Lee, A non-Fermi liquid from a charged black hole: A critical Fermi ball, Phys. Rev. D **79**, 086006 (2009).

[34] O. Bergman, N. Jokela, G. Lifschytz, and M. Lippert, Striped instability of a holographic Fermi-like liquid, J. High Energy Phys. 10 (2011) 034.

[35] R. A. Davison, M. Goykhman, and A. Parnachev, AdS/CFT and Landau Fermi liquids, J. High Energy Phys. 07 (2014) 109.

[36] S. Bhattacharyya, S. Lahiri, R. Loganayagam, and S. Minwalla, Large rotating AdS black holes from fluid mechanics, J. High Energy Phys. 09 (2008) 054.

[37] S. Bhattacharyya, V. E. Hubeny, S. Minwalla, and M. Rangamani, Nonlinear fluid dynamics from gravity, J. High Energy Phys. 02 (2008) 045.

[38] S. Bhattacharyya, V. E. Hubeny, R. Loganayagam, G. Mandal, S. Minwalla, T. Morita, M. Rangamani, and H. S. Reall, Local fluid dynamical entropy from gravity, J. High Energy Phys. 06 (2008) 055.

[39] I. Bredberg, C. Keeler, V. Lysov, and A. Strominger, Wilsonian approach to fluid/gravity duality, J. High Energy Phys. 03 (2011) 141.

[40] I. Bredberg, C. Keeler, V. Lysov, and A. Strominger, From Navier-Stokes to Einstein, J. High Energy Phys. 07 (2012) 146.

[41] G. Policastro, D. T. Son, and A. O. Starinets, From AdS/CFT correspondence to hydrodynamics, J. High Energy Phys. 09 (2002) 043.
[42] G. Policastro, D. T. Son, and A. O. Starinets, From AdS/CFT correspondence to hydrodynamics. 2. Sound waves, J. High Energy Phys. 12 (2002) 054.
[43] C. P. Herzog, The Hydrodynamics of M theory, J. High Energy Phys. 12 (2002) 026.
[44] C. P. Herzog, The Sound of M theory, Phys. Rev. D **68**, 024013 (2003).
[45] P. Kovtun, D. T. Son, and A. O. Starinets, Holography and hydrodynamics: Diffusion on stretched horizons, J. High Energy Phys. 10 (2003) 064.
[46] P. Kovtun, D. T. Son, and A. O. Starinets, Viscosity in Strongly Interacting Quantum Field Theories from Black Hole Physics, Phys. Rev. Lett. **94**, 111601 (2005).
[47] D. T. Son and A. O. Starinets, Viscosity, black holes, and quantum field theory, Annu. Rev. Nucl. Part. Sci. **57**, 95 (2007).
[48] J. P. S. Lemos, Cylindrical black hole in general relativity, Phys. Lett. B **353**, 46 (1995).
[49] J. P. S. Lemos and V. T. Zanchin, Rotating charged black string and three-dimensional black holes, Phys. Rev. D **54**, 3840 (1996).
[50] J. Stachel, Globally stationary but locally static spacetimes: A gravitational analog of the Aharonov-Bohm effect, Phys. Rev. D **26**, 1281 (1982).
[51] D. T. Son and A. O. Starinets, Minkowski-space correlators in AdS/CFT correspondence: Recipe and applications, J. High Energy Phys. 09 (2002) 042.
[52] C. P. Herzog and D. T. Son, Schwinger-Keldysh propagators from AdS/CFT correspondence, J. High Energy Phys. 03 (2003) 046.
[53] K. Skenderis and B. C. van Rees, Real-Time Gauge/Gravity Duality, Phys. Rev. Lett. **101**, 081601 (2008).
[54] K. Skenderis and B. C. van Rees, Real-time gauge/gravity duality: Prescription, renormalization, and examples, J. High Energy Phys. 05 (2009) 085.
[55] V. Cardoso and J. P. S. Lemos, Scalar, electromagnetic and Weyl perturbations of BTZ black holes: Quasinormal modes, Phys. Rev. D **63**, 124015 (2001).
[56] D. Birmingham, I. Sachs, and S. N. Solodukhin, Conformal Field Theory Interpretation of Black Hole Quasinormal Modes, Phys. Rev. Lett. **88**, 151301 (2002).
[57] D. Birmingham, I. Sachs, and S. N. Solodukhin, Relaxation in conformal field theory, Hawking-Page transition, and quasinormal normal modes, Phys. Rev. D **67**, 104026 (2003).
[58] K. D. Kokkotas and B. G. Schmidt, Quasinormal modes of stars and black holes, Living Rev. Relativity **2**, 2 (1999).
[59] H. P. Nollert, Topical review: Quasinormal modes: the characteristic 'sound' of black holes and neutron stars, Classical Quantum Gravity **16**, R159 (1999).
[60] G. T. Horowitz and V. E. Hubeny, Quasinormal modes of AdS black holes and the approach to thermal equilibrium, Phys. Rev. D **62**, 024027 (2000).
[61] V. Cardoso and J. P. S. Lemos, Quasi-normal modes of Schwarzschild anti-de Sitter black holes: Electromagnetic and gravitational perturbations, Phys. Rev. D **64**, 084017 (2001).
[62] A. Nunez and A. O. Starinets, AdS/CFT correspondence, quasinormal modes, and thermal correlators in $N = 4$ SYM, Phys. Rev. D **67**, 124013 (2003).
[63] P. K. Kovtun and A. O. Starinets, Quasinormal modes and holography, Phys. Rev. D **72**, 086009 (2005).
[64] E. Berti, V. Cardoso, and A. O. Starinets, Quasinormal modes of black holes and black branes, Classical Quantum Gravity **26**, 163001 (2009).
[65] R. A. Konoplya and A. Zhidenko, Quasinormal modes of black holes: From astrophysics to string theory, Rev. Mod. Phys. **83**, 793 (2011).
[66] A. O. Starinets, Quasinormal modes of near extremal black branes, Phys. Rev. D **66**, 124013 (2002).
[67] V. Cardoso and J. P. S. Lemos, Quasinormal modes of toroidal, cylindrical and planar black holes in anti-de Sitter space-times, Classical Quantum Gravity **18**, 5257 (2001).
[68] A. S. Miranda and V. T. Zanchin, Quasinormal modes of plane-symmetric anti-de Sitter black holes: A complete analysis of the gravitational perturbations, Phys. Rev. D **73**, 064034 (2006).
[69] A. S. Miranda and V. T. Zanchin, Gravitational perturbations and quasinormal modes of black holes with non-spherical topology, Int. J. Mod. Phys. D **16**, 421 (2007).
[70] A. S. Miranda, J. Morgan, and V. T. Zanchin, Quasinormal modes of plane-symmetric black holes according to the AdS/CFT correspondence, J. High Energy Phys. 11 (2008) 030.
[71] J. Morgan, V. Cardoso, A. S. Miranda, C. Molina, and V. T. Zanchin, Quasinormal modes of black holes in anti-de Sitter space: A Numerical study of the eikonal limit, Phys. Rev. D **80**, 024024 (2009).
[72] J. Morgan, V. Cardoso, A. S. Miranda, C. Molina, and V. T. Zanchin, Gravitational quasinormal modes of AdS black branes in d spacetime dimensions, J. High Energy Phys. 09 (2009) 117.
[73] J. Morgan, A. S. Miranda, and V. T. Zanchin, Electromagnetic quasinormal modes of rotating black strings and the AdS/CFT correspondence, J. High Energy Phys. 03 (2013) 169.
[74] M. M. Caldarelli, O. J. C. Dias, and D. Klemm, Dyonic AdS black holes from magnetohydrodynamics, J. High Energy Phys. 03 (2009) 025.
[75] V. Cardoso, O. J. C. Dias, G. S. Hartnett, L. Lehner, and J. E. Santos, Holographic thermalization, quasinormal modes and superradiance in Kerr-AdS, J. High Energy Phys. 04 (2014) 183.
[76] O. Semerák, Stationary frames in the Kerr field, Gen. Relativ. Gravit. **25**, 1041 (1993).
[77] C. W. Misner, J. A. Wheeler, and K. S. Thorne, *Gravitation* (W. H. Freeman, San Francisco, 1973).
[78] A. M. Awad, Higher dimensional charged rotating solutions in (A)dS space-times, Classical Quantum Gravity **20**, 2827 (2003).
[79] M. Visser, The Kerr spacetime: A brief introduction, arXiv:0706.0622.
[80] A. S. Miranda, J. Morgan, V. T. Zanchin, and A. Kandus, Separable wave equations for gravitoelectromagnetic perturbations of rotating charged black strings, Classical Quantum Gravity **32**, 235002 (2015).

[81] G. Michalogiorgakis and S. S. Pufu, Low-lying gravitational modes in the scalar sector of the global AdS(4) black hole, J. High Energy Phys. 02 (2007) 023.
[82] Ó. J. C. Dias and J. E. Santos, Boundary conditions for Kerr-AdS perturbations, J. High Energy Phys. 10 (2013) 156.
[83] J. Noronha and G. S. Denicol, Transient fluid dynamics of the quark-gluon plasma according to AdS/CFT, arXiv: 1104.2415.
[84] M. P. Heller, R. A. Janik, M. Spalinski, and P. Witaszczyk, Coupling Hydrodynamics to Nonequilibrium Degrees of Freedom in Strongly Interacting Quark-Gluon Plasma, Phys. Rev. Lett. **113**, 261601 (2014).
[85] R. A. Janik, AdS/CFT for the early stages of heavy ion collisions, Nucl. Phys. **A931**, 176 (2014).
[86] W. Witczak-Krempa and S. Sachdev, Dispersing quasinormal modes in $2+1$ dimensional conformal field theories, Phys. Rev. B **87**, 155149 (2013).
[87] G. B. Cook and M. Zalutskiy, Purely imaginary quasinormal modes of the Kerr geometry, Classical Quantum Gravity **33**, 245008 (2016).
[88] G. B. Cook and M. Zalutskiy, Modes of the Kerr geometry with purely imaginary frequencies, Phys. Rev. D **94**, 104074 (2016).
[89] S. I. Finazzo, R. Rougemont, M. Zaniboni, R. Critelli, and J. Noronha, Critical behavior of non-hydrodynamic quasinormal modes in a strongly coupled plasma, J. High Energy Phys. 01 (2017) 137.
[90] S. Chandrasekhar, On algebraically special perturbations of black holes, Proc. R. Soc. A **392**, 1 (1984).
[91] G. Chee, Note on a solution of the algebraically special perturbation of the Schwarzschild black hole, J. Math. Phys. (N.Y.) **35**, 3025 (1994).
[92] A. Maassen van den Brink, Analytic treatment of black hole gravitational waves at the algebraically special frequency, Phys. Rev. D **62**, 064009 (2000).
[93] W. E. Couch and E. T. Newman, Algebraically special perturbations of the Schwarzschild metric, J. Math. Phys. (N.Y.) **14**, 285 (1973).
[94] R. M. Wald, On perturbations of a Kerr black hole, J. Math. Phys. (N.Y.) **14**, 1453 (1973).
[95] H. Onozawa, Detailed study of quasinormal frequencies of the Kerr black hole, Phys. Rev. D **55**, 3593 (1997).
[96] E. Berti, V. Cardoso, K. D. Kokkotas, and H. Onozawa, Highly damped quasinormal modes of Kerr black holes, Phys. Rev. D **68**, 124018 (2003).
[97] O. J. C. Dias and H. S. Reall, Algebraically special perturbations of the Schwarzschild solution in higher dimensions, Classical Quantum Gravity **30**, 095003 (2013).
[98] J. D. Jackson, *Classical Electrodynamics* (John Wiley & Sons, New York, 1998).
[99] J. M. Houlrik, The relativistic wave vector, Eur. J. Phys. **30**, 777 (2009).
[100] A. Haber, A. Schmitt, and S. Stetina, Instabilities in relativistic two-component (super)fluids, Phys. Rev. D **93**, 025011 (2016).
[101] L. P. Kanadoff and P. C. Martin, Hydrodynamic equations and correlation functions, Ann. Phys. (N.Y.) **24**, 419 (1963).